

RESEARCH ARTICLE

# Weakening the tight coupling between geometry and simulation in isogeometric analysis: From sub- and super-geometric analysis to Geometry-Independent Field approximation (GIFT)

Elena Atroshchenko<sup>1</sup>  | Satyendra Tomar<sup>2</sup>  | Gang Xu<sup>3</sup>  | Stéphane P.A. Bordas<sup>2,4</sup> 

<sup>1</sup>Department of Mechanical Engineering, University of Chile, Santiago, Chile

<sup>2</sup>Institute of Computational Engineering, Faculty of Sciences Communication and Technology, University of Luxembourg, Luxembourg City, Luxembourg

<sup>3</sup>Hangzhou Dianzi University, Hangzhou, China

<sup>4</sup>Institute of Mechanics and Advanced Materials, School of Engineering, Cardiff University, Cardiff, UK

## Correspondence

Stéphane P.A. Bordas, Institute of Computational Engineering, Faculty of Sciences Communication and Technology, University of Luxembourg, Luxembourg City, Luxembourg; Institute of Mechanics and Advanced Materials, School of Engineering, Cardiff University, Cardiff, UK; Intelligent Systems for Medicine Laboratory, University of Western Australia, Perth, Australia.  
Email: stephane.bordas@uni.lu

## Funding information

University of Luxembourg; European Research Council Starting Independent Research Grant, Grant/Award Number: 279578; Luxembourg National Research Funds, Grant/Award Number: INTER/FWO/15/10318764 and INTER/MOBILITY/14/8813215/CBM/Bordas; National Nature Science Foundation of China, Grant/Award Number: 61772163 and 61472111; Zhejiang Provincial Natural Science Foundation of China, Grant/Award Number: LR16F020003, LQ16F020005, Open Project Program of the State Key Lab of CAD&CG and A1703

## Summary

This paper presents an approach to generalize the concept of isogeometric analysis by allowing different spaces for the parameterization of the computational domain and for the approximation of the solution field. The method inherits the main advantage of isogeometric analysis, ie, preserves the original exact computer-aided design geometry (for example, given by nonuniform rational B-splines), but allows pairing it with an approximation space, which is more suitable/flexible for analysis, for example, T-splines, LR-splines, (truncated) hierarchical B-splines, and PHT-splines. This generalization offers the advantage of adaptive local refinement without the need to reparameterize the domain, and therefore without weakening the link with the computer-aided design model. We demonstrate the use of the method with different choices of geometry and field spaces and show that, despite the failure of the standard patch test, the optimum convergence rate is achieved for nonnested spaces.

## KEYWORDS

CAD, IGA, NURBS, PHT-splines

## 1 | INTRODUCTION

### 1.1 | Contribution

We present an approach that enables the use of separate approximation spaces for the field and geometry in isogeometric finite element methods. For example, coarse nonuniform rational B-splines (NURBS) approximations can be used for the geometry, and locally adapted PHT-splines can be used for the field variables. This endows the method with flexibility to locally enrich the approximation space for the field variables without modifying the space used for the parameterization of the domain geometry. We verify the approach with various parameterizations of the geometry and approximations of the field variables and on 2- and 3-dimensional geometries. We give a detailed mathematical explanation on the ability of the resulting method to pass the patch test and to converge with an optimal rate. Geometry-Independent Field approximation (GIFT), as we coined the approach, represents a simple and computationally efficient alternative to isogeometric analysis (IGA), which preserves the tight integration with computer-aided design (CAD) and allows adaptive local refinement of the solution field.

### 1.2 | Background

Isogeometric analysis was introduced in the work of Hughes et al<sup>1</sup> to establish a direct link between CAD and the analysis. Over the last decade, fuelled by rapid developments in computer graphics and CAD and because of a number of advantages offered by spline basis functions over standard Lagrange basis functions in finite element analysis (FEA), such as higher continuity, exact representation of the geometry, simplified integration, and their behavior in dynamics, IGA has generated a huge interest in computational engineering and science.

The method has found many applications in various areas such as structural vibrations,<sup>2</sup> fluid-structure interaction,<sup>3</sup> shell analysis,<sup>4</sup> and fracture mechanics.<sup>5</sup> Although the finite element version of IGA suffers from significant difficulties associated with generating volumetric parameterizations directly from CAD, coupling IGA with boundary element methods enables the performance of computations directly from the CAD description of the boundary of the domain.<sup>6</sup> Applications include stress analysis,<sup>7-9</sup> shape optimization,<sup>10-12</sup> fracture mechanics,<sup>13-15</sup> geomechanics,<sup>16</sup> acoustics,<sup>17,18</sup> and electromagnetics.<sup>19</sup> A detailed overview of the recent work in the field can be found in the works of Nguyen et al<sup>20</sup> and Lian et al.<sup>21</sup>

### 1.3 | NURBS: Advantages and limitations

Nonuniform rational B-splines are the most common type of splines used in the CAD industry to describe geometry. NURBS shape functions are defined by means of B-splines (piecewise polynomial functions defined over a knot vector) and a set of control points with associated weights. The main feature of NURBS is the ability to exactly represent conic sections, eg. ellipses, parabolas, and hyperbolas, which are widely used in CAD. Furthermore, NURBS basis functions also possess all the properties of the standard FEM basis functions such as compact support, linear independence, and partition of unity. Moreover, the high-order continuity ( $C^{p-k}$ , with  $p$  as the polynomial order and  $k$  as the knot repetition) of NURBS basis functions across elements facilitates the solution of partial differential equations of arbitrary high order. However, NURBS are based on tensor product structure, which does not facilitate local refinement (see Figure 2A), and the use of NURBS may result in producing “gaps” in geometries for general shapes. This imposes difficulties for mesh generation, and requires coupling algorithms for multipatch geometries.<sup>22-25</sup>

### 1.4 | Motivation

The main idea of IGA is to use the same shape functions (splines) for both, the parameterization of the geometry (computational domain) and the approximation of the unknown solution (see Figure 1). This is a clear advantage in engineering design, as any modification of the CAD geometry is directly inherited by the approximation of the unknown fields so that the mesh need not be regenerated at each iteration of the geometrical design process. Because of the most commonly used functions in geometrical design (NURBS), which are based on tensor product constructions, the potential power of IGA may not be fully harnessed in simulation practices. Indeed, local refinement is not natural in NURBS approximations. Moreover, situations usually arise when the approximation used for the field variables must be locally refined whilst keeping the same (coarser) geometrical approximation. This is the case in shape optimization<sup>10-12</sup> or for

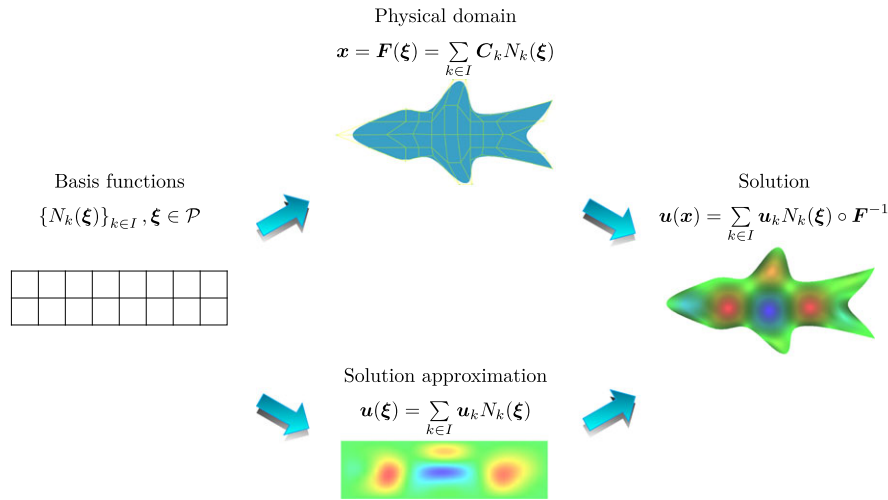


**FIGURE 1** Main idea of the isogeometric analysis: the same shape functions are used for geometry parameterization and solution approximation. For the notations, see Section 2 [Colour figure can be viewed at [wileyonlinelibrary.com](http://wileyonlinelibrary.com)]

problems with singularities, boundary layers, or steep gradients. In the work of Schillinger et al,<sup>26</sup> an isogeometric design-through-analysis based on adaptive hierarchical refinement of NURBS was presented in detail. In this article, however, the adaptivity is based on the a priori knowledge of regions of interest, and is not based on error estimation.

It appears, therefore, that it is useful to develop more general methods where the approximation space used for the geometry and that used for the field variables be decoupled. The investigation of the behavior of such methods for the linear elasticity and Laplace equation is the focus of this paper. We base our work on the developments made by the team of Gernot Beer in an important paper for isogeometric boundary element methods,<sup>27</sup> which was further developed in a series of papers targeting geomechanics and fluid mechanics problems.<sup>16,28-31</sup>

The most important shortcomings of IGA, which served as motivation to investigate the possibility to decouple the geometry and the solution fields, can be summarized as follows.

1. The  $h$ - and  $p$ -refinements of the original exact geometry is redundant in IGA. For large industrial problems, the computational savings for only refining the solution space while keeping the geometry representation fixed is expected to be significant.
2. In addition, NURBS, the de facto standard in the CAD community, does not offer local refinement. Therefore, in order to use any other locally refined splines with the original CAD model given by NURBS, staying within the isoparametric concept will require a reparameterization of the original geometry. Note that some locally refined splines (eg, T-splines) allow the exact representation of the original geometry, but others (eg, polynomial based splines) do not offer this advantage. Therefore, such operations (particularly, for efficient local refinement) are not only time consuming but also may lead to losing the geometry exactness, and may introduce the need to communicate with the CAD model at every step of the solution refinement process.

## 1.5 | Alternatives to NURBS

In many applications, the efficiency of a numerical method can be drastically improved by restricting the refinement to certain areas (for example, where the solution exhibits steep gradients). Therefore, the local refinement issue in IGA is currently an active research topic. A recent survey on locally refinable splines is given in the work of Li et al.<sup>32</sup> In the authors' opinion, the most commonly used alternatives that allow local refinement are THB-splines (truncated hierarchical B-splines), T-splines, and PHT-splines (polynomial splines over hierarchical T-meshes), which are briefly discussed below.

### 1.5.1 | Hierarchical B-splines and truncated hierarchical B-splines (THB-splines)

Hierarchical B-splines were first introduced in the work of Forsey and Bartels<sup>33</sup> for surface fitting. They possess such properties as maximum continuity on each refinement level and linear independence of the basis functions. Later, in the

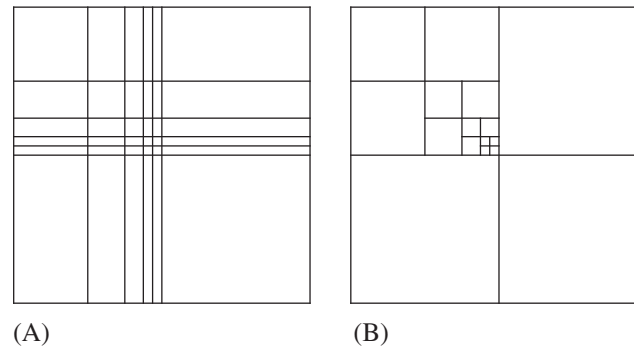


**FIGURE 2** Refinements in the parametric space. A, Tensor product mesh in the parametric space (global refinement); B, T-mesh in the parametric space (local refinement)

work of Vuong et al,<sup>34</sup> these shape functions were modified to reduce the local support and assure the partition of unity property. These splines were called THB-splines. The theoretical background, as well as applications to isogeometrical analysis, can be found in the works of Giannelli et al.<sup>35,36</sup>

### 1.5.2 | T-splines

T-splines, introduced by Sederberg et al,<sup>37,38</sup> are defined over so-called T-meshes (see Figure 2B). T-splines are piecewise rational functions, which preserve the exactness of the NURBS geometry. Moreover, a multipatch NURBS geometry parameterization can be converted into a single patch T-splines description without gaps and leaks. However, in the most general case, the linear independence of T-splines blending functions is not guaranteed, and this led to the introduction of so-called analysis-suitable T-splines.<sup>39,40</sup> The analysis-suitable T-splines have been successfully applied to IGA, see, eg, the work of da Veiga et al.<sup>41</sup> In a recent paper by Zhang and Li,<sup>42</sup> the degree elevation of T-splines have also been studied. However, as described in the work of Scott et al,<sup>43</sup> the implementation, particularly the algorithm of knot insertion that preserves analysis suitability, is complicated.

### 1.5.3 | PHT-splines

PHT-splines were introduced by Deng et al in 2008.<sup>44</sup> In addition to the main properties of B-splines, the main advantage of PHT-splines, which makes them attractive for IGA, is an efficient and simple refinement algorithm.<sup>45</sup> However, the tradeoff is the reduced continuity ( $C^1$ ). Nevertheless, this is enough for most applications in solid and structural mechanics. Since PHT-splines are polynomials, the CAD geometry of arbitrary topology may not be represented exactly, which led to the development of rational PHT-splines.<sup>46</sup>

### 1.5.4 | Geometric design and IGA considerations for unstructured quadrilateral meshes

Recently, Toshniwal et al<sup>47</sup> proposed a new framework for the geometric design and IGA on unstructured quadrilateral meshes  $M$ . Following the construction of D-patch framework developed in the work of Reif,<sup>48</sup> and the construction of  $C^1$  smooth spline elements in the neighborhood of extraordinary points (albeit only for PHT-splines) in the work of Nguyen and Peters,<sup>49</sup> the focus of the work of Toshniwal et al<sup>47</sup> is on the construction of smooth, linearly independent, and locally supported spline functions over  $M$ . To achieve the smoothness at the extraordinary points, affine-invariant linear transformations (called *smoothing matrices*) from the work of Reif<sup>48</sup> are employed. As oppose to the work of Nguyen and Peters,<sup>49</sup> the work of Toshniwal et al<sup>47</sup> uses the smoothing matrices with nonnegative coefficients. Although it yields higher-quality surfaces for geometric modeling applications, this comes at the cost of slight (very small) variations in geometries during the refinement. The design and analysis spline spaces are then simply defined as the span of these splines. The design space  $S_D$  is contained within the analysis space  $S_A$  at  $k = 0$  (the coarsest level for analysis), and under the assumption of idempotence of the smoothing matrices, the spaces  $S_A^k$  are nested, ie,  $S_D \subseteq S_A =: S_A^0 \subseteq S_A^1 \subseteq S_A^2 \cdots \subseteq S_A^k$ . For isogeometric compatibility, simple transformation rules for change of basis from  $S_D$  to  $S_A$  are constructed.

### 1.6 | Generalizing the isogeometric concept

In this paper, instead of aiming to construct tailored spline spaces for dealing with local refinement and/or unstructured meshes, we aim to generalize the isogeometric concept, namely, to possibly choose different spaces for design and analysis (where  $S_D$  may not be contained in  $S_A$ ). Thereby, while remaining in the realm of existing technologies for design, we can use suitable spline spaces for analysis.

In order to preserve the isogeometric concept, with the 3 choices of splines described previously, it is required to convert the original NURBS CAD geometry to a parameterization (exact or approximate) in the same spline space. This contradicts the original objective of the IGA to bring the direct link between the CAD design and analysis. This limitation, caused by tight integration of the geometry parameterization and the approximation of the solution (Figure 1) in IGA, motivated the authors to formulate a generalized approach: **Geometry-Independent Field approximaTion (GIFT)**. The main idea of GIFT is to retain the original CAD geometry whilst flexibly adapting the solution basis to best fit the solution field (Figure 3). For example, a NURBS geometry can be used together with a PHT-spline approximation for the solution.

The main features of GIFT can be summarized as follows:

- preserve exact CAD geometry (provided in any form, including B-splines or NURBS) at any stage of the solution process;
- allow local refinement of the solution by choosing appropriate field approximations, as independently as possible of the geometrical parameterization of the domain, including partition of unity enrichment; and
- exploit computational savings by not refining the geometry during the solution refinement process, and by choosing simpler approximations for the solution, ie, polynomial functions instead of rational functions.

This paper aims at showing a proof of concept for GIFT. We present the general framework of the method, followed by patch test studies, which is then followed by a number of numerical examples. In our implementation of GIFT, the geometry is given by NURBS because this is the most commonly used form of geometry description in CAD. For solution approximations, we use a variety of functions spaces, including NURBS (with potentially different degrees and knot vectors compared to those used for the geometry), PHT-splines, and B-splines.

*Remark 1.* In the engineering community, such different choices of spline spaces for geometry and field give rise to the question of verification of the patch test. The role of the patch test in the convergence of the finite element-based method is a long standing debate. It has been shown in the work of Stummel<sup>50</sup> that, for the method to converge with an optimal rate, the patch test is neither sufficient nor necessary. The present study also investigates the relation of the convergence properties of the method with the standard patch test. The spline spaces for the geometry and the field are chosen such that they may or may not pass the patch test, yet the numerical results show optimal convergence rates.

The organization of the remainder of this article is as follows. We first present a simple introduction to the mathematical formulation of GIFT in Section 2. In Section 3, we present the study of various patch tests. The numerical examples on

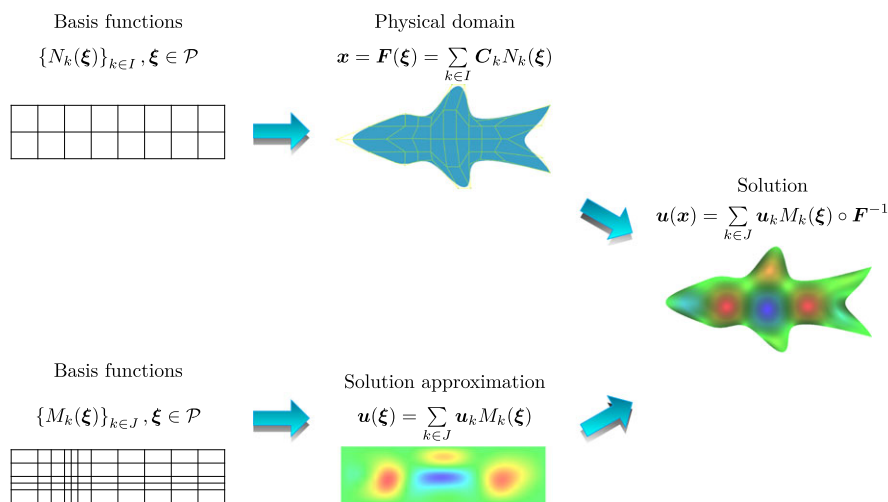


**FIGURE 3** Main idea of Geometry-Independent Field approximaTion: different shape functions are used for geometry parameterization and solution approximation. For the notations, see Section 2 [Colour figure can be viewed at wileyonlinelibrary.com]

convergence studies are presented in Section 4. These patch tests and numerical examples are carefully designed to study various combinations of bases for geometry and solution approximation. Finally, some conclusions and recommendations for future work are outlined in Section 5.

## 2 | FORMULATION OF GIFT

We consider an open domain  $\Omega \subset \mathbb{R}^d$ ,  $d \geq 2$ , with boundary  $\Gamma$  consisting of 2 parts  $\Gamma_D$  and  $\Gamma_N$  such that:  $\Gamma = \overline{\Gamma_D \cup \Gamma_N}$ ,  $\Gamma_D \cap \Gamma_N = \emptyset$ . The domain  $\Omega$  is parameterized on a parametric domain  $\mathcal{P}$  by mapping  $F$  as follows:

$$F : \mathcal{P} \rightarrow \Omega, \quad \mathbf{x} = F(\xi), \quad \mathbf{x} \in \Omega, \quad \xi \in \mathcal{P}. \quad (1)$$

In what follows, we will denote the NURBS basis by  $\mathcal{N}_{i,j}$ , and the B-splines basis by  $\mathcal{B}_{i,j}$ , with  $i$  denoting the degree in the  $\xi$  direction and  $j$  denoting the degree in the  $\eta$  direction. Typically, the geometrical map  $F$  is given by a set of basis functions  $N_{i_1, i_2, \dots, i_d}(\xi)$  and a set of control points  $\mathbf{C}_{i_1, i_2, \dots, i_d}$  as

$$F(\xi) = \sum_{i_1=1}^{n_1} \sum_{i_2=1}^{n_2} \cdots \sum_{i_d=1}^{n_d} \mathbf{C}_{i_1, i_2, \dots, i_d} N_{i_1, i_2, \dots, i_d}(\xi), \quad (2)$$

where  $N_{i_1, i_2, \dots, i_d}(\xi)$  can be a tensor product of NURBS, B-splines, T-splines, PHT-splines, etc. For brevity reasons, we introduce 2 sets of multi-indices  $(i_1, i_2, \dots, i_d)$  of NURBS basis functions by

$$\mathbf{I} = \{(i_1, i_2, \dots, i_d) : i_1 \in \{1, \dots, n_1\}, \dots, i_d \in \{1, \dots, n_d\}\} \quad (3a)$$

$$\mathbf{J} = \{(i_1, i_2, \dots, i_d) : i_1 \in \{1, \dots, m_1\}, \dots, i_d \in \{1, \dots, m_d\}\}. \quad (3b)$$

Moreover, wherever suitable, for multi-index  $(i_1, i_2, \dots, i_d)$ , we will interchangeably use the collapsed notation  $\mathbf{k}$ . Thence, Equations (1) and (2) are written as

$$\mathbf{x}(\xi) = \sum_{\mathbf{k} \in \mathbf{I}} \mathbf{C}_{\mathbf{k}} N_{\mathbf{k}}(\xi). \quad (4)$$

In what follows, we will refer to the set  $\{N_{\mathbf{k}}(\xi)\}_{\mathbf{k} \in \mathbf{I}}$  as the *geometry basis*. For change of variables, we will also need the Jacobian matrix  $J(\xi)$  of the mapping  $F$ , which is given by

$$J_{ij}(\xi) = \frac{\partial x_i}{\partial \xi_j}(\xi) = \sum_{\mathbf{k} \in \mathbf{I}} \mathbf{C}_{\mathbf{k}i} \frac{\partial N_{\mathbf{k}}(\xi)}{\partial \xi_j}. \quad (5)$$

The departure from the classical isogeometric analysis consists in choosing a *solution basis*  $\{M_{\mathbf{k}}(\xi)\}_{\mathbf{k} \in \mathbf{J}}$ , which is different from the geometry basis, and looking for the solution in the following form:

$$u(\xi) = \sum_{\mathbf{k} \in \mathbf{J}} u_{\mathbf{k}} M_{\mathbf{k}}(\xi), \quad (6)$$

where  $u_{\mathbf{k}}$  are the unknown control variables. In order to evaluate derivatives of the solution basis function  $M_{\mathbf{k}}(\xi)$  with respect to variables  $\mathbf{x}$ , the standard chain rule is used, which, in 2 dimensions, read as follows:

$$\begin{pmatrix} \frac{\partial M_{\mathbf{k}}(\xi, \eta)}{\partial x} \\ \frac{\partial M_{\mathbf{k}}(\xi, \eta)}{\partial y} \end{pmatrix} = \begin{pmatrix} \frac{\partial \xi}{\partial x} & \frac{\partial \eta}{\partial x} \\ \frac{\partial \xi}{\partial y} & \frac{\partial \eta}{\partial y} \end{pmatrix} \begin{pmatrix} \frac{\partial M_{\mathbf{k}}(\xi, \eta)}{\partial \xi} \\ \frac{\partial M_{\mathbf{k}}(\xi, \eta)}{\partial \eta} \end{pmatrix}. \quad (7)$$

In matrix notations (independent of dimensions), this can be written as follows:

$$\nabla_{\mathbf{x}} M_{\mathbf{k}}(\xi) = J^{-T}(\xi) \nabla_{\xi} M_{\mathbf{k}}(\xi), \quad (8)$$

where  $J^{-T}(\xi)$  is the transpose of the inverse of the Jacobian matrix (5).

Now, let the weak form of the boundary value problem be given by

$$a(u, v) = \ell(v). \quad (9)$$

By substituting Equations (4) and (6) into (9), we obtain the linear system of equations as

$$\mathbf{K} \mathbf{u} = \mathbf{f}, \quad (10)$$

where the stiffness matrix  $\mathbf{K}$  and the force vector  $\mathbf{f}$  are given by

$$\mathbf{K}_{ij} = a(M_i(\mathbf{x}), M_j(\mathbf{x})), \quad \mathbf{f}_i = \ell(M_i(\mathbf{x})), \quad (11)$$

and vector  $\mathbf{u}$  consists of all unknown control variables  $u_j$ .

The error  $e$  between the exact solution  $u_{\text{exact}}(\mathbf{x})$  and the numerical solution  $u(\mathbf{x})$  is defined as

$$e = |u_{\text{exact}}(\mathbf{x}) - u(\mathbf{x})|, \quad (12)$$

and the  $L^2$  error norm is given by

$$\|e\|_{L^2(\Omega)} = \left( \int_{\Omega} |u_{\text{exact}}(\mathbf{x}) - u(\mathbf{x})|^2 d\Omega \right)^{1/2}. \quad (13)$$

For our numerical results, we consider two problems, namely, Poisson's equation and the problem of linear elasticity. In Sections 2.1 and 2.2, we briefly describe the weak form of these problems.

## 2.1 | Poisson's equation

For the Poisson's problem, the terms in the weak form are defined as

$$a(u, v) = \int_{\Omega} \nabla u \cdot \nabla v d\Omega, \quad \ell(v) = \int_{\Omega} f v d\Omega + \int_{\partial\Omega_N} g v d\Gamma, \quad (14)$$

where  $f$  is the source function and  $g$  is the flux prescribed on Neumann part of the boundary. Equation (11) thus results in, for  $i, j = 1, \dots, M$ ,

$$\begin{aligned} \mathbf{K}_{ij} &= \int_{\Omega} \nabla_x M_i(\mathbf{x}) \cdot \nabla_x M_j(\mathbf{x}) d\Omega, \\ \mathbf{f}_i &= \int_{\Omega} f(\mathbf{x}) M_i(\mathbf{x}) d\Omega + \int_{\partial\Omega_N} g(\mathbf{x}) M_i(\mathbf{x}) d\Gamma. \end{aligned} \quad (15)$$

## 2.2 | Linear elasticity

Consider the linear elasticity problem in two dimensions, for which the weak form is given by

$$a(u, v) = \int_{\Omega} \boldsymbol{\epsilon}(u)^T \mathbf{D} \boldsymbol{\epsilon}(v) d\Omega, \quad \ell(v) = \int_{\Omega} f v d\Omega + \int_{\partial\Omega_N} \tilde{t} v d\Gamma, \quad (16)$$

where  $\mathbf{u} := (u_x, u_y)^T$  denotes the vector of unknown displacements,  $f$  denotes the body forces,  $\tilde{t}$  denotes the tractions prescribed on Neumann boundary, and the matrix of material parameters in the plane strain is given by

$$\mathbf{D} = \frac{E}{(1+\nu)(1-2\nu)} \begin{pmatrix} 1-\nu & \nu & 0 \\ \nu & 1-\nu & 0 \\ 0 & 0 & (1-2\nu)/2 \end{pmatrix}, \quad (17)$$

where  $E$  is the Young's modulus and  $\nu$  is the Poisson's coefficient. The strain operator, which is defined as

$$\boldsymbol{\epsilon}(u) = \begin{pmatrix} \partial u_x / \partial x \\ \partial u_y / \partial y \\ \partial u_x / \partial y + \partial u_y / \partial x \end{pmatrix}, \quad (18)$$

applied to the solution approximation given by Equation (6), yields the following stiffness matrix and force vector:

$$\begin{aligned} \mathbf{K}_{ij} &= \int_{\Omega} \mathbf{B}_i^T \mathbf{D} \mathbf{B}_j d\Omega, \\ \mathbf{f}_i &= \int_{\Omega} f(\mathbf{x}) M_i(\mathbf{x}) d\Omega + \int_{\partial\Omega_N} \tilde{t}(\mathbf{x}) M_i(\mathbf{x}) d\Gamma, \end{aligned} \quad (19)$$

where the strain operator  $\mathbf{B}_i$  is defined as

$$\mathbf{B}_i = \begin{pmatrix} \frac{\partial M_i(\xi, \eta)}{\partial x} & 0 \\ 0 & \frac{\partial M_i(\xi, \eta)}{\partial y} \\ \frac{\partial M_i(\xi, \eta)}{\partial y} & \frac{\partial M_i(\xi, \eta)}{\partial x} \end{pmatrix}, \quad (20)$$

and the derivatives of the solution shape functions with respect to geometry variables are evaluated according to Equation (7).

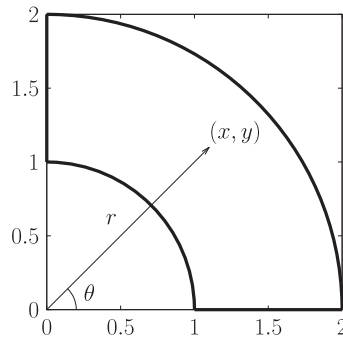


**FIGURE 4** Quarter annulus

### 3 | PATCH TESTS

In this section, we will study the classical patch test for various combinations of bases for the geometry representation and the solution approximation. For all the test cases, we will study two problems, namely, the Laplace equation and linear elasticity problem, which are defined in Section 3.1. We present the analysis of the patch test results (including the values of the field control variables). This can also serve as a guide for engineers to design patch tests in spline-based methods.

#### 3.1 | Problem definition

We formulate two problems in a quarter annulus domain  $\Omega$ , as shown in Figure 4. The first problem is for the two-dimensional Laplace equation, where we use the linear solution

$$u(x, y) = 1 + x + y, \quad (21)$$

imposed as the Dirichlet boundary condition on the entire boundary  $\partial\Omega$ , ie,

$$\begin{aligned} \Delta u &= 0, \quad \text{in } \Omega \\ u|_{\partial\Omega}(x, y) &= 1 + x + y. \end{aligned} \quad (22)$$

The second problem is for the linear elasticity, which is given in polar coordinates  $(r, \theta)$  by

$$\begin{aligned} \sigma_{ij,j} &= 0, & \text{in } \Omega \\ t_i &= \sigma_0 n_i, & \text{at } r = 1, 2, \\ u_y = 0, \quad t_x &= 0, & \text{at } \theta = 0, \\ u_x = 0, \quad t_y &= 0, & \text{at } \theta = \pi/2, \end{aligned} \quad (23)$$

where  $i$  and  $j$  represent both the variables  $x$  and  $y$ . This admits a linear solution (a plane strain case), which is given by

$$u_x(x) = \frac{(1+\nu)(1-2\nu)}{E} \sigma_0 x, \quad u_y(y) = \frac{(1+\nu)(1-2\nu)}{E} \sigma_0 y, \quad (24)$$

where  $\sigma_0$  is the pressure applied to the inner and outer side of the cylinder (equal on both sides in order to produce a linear solution).

#### 3.2 | Geometry parameterization

As shown in Figure 5, the coarsest parameterization of the quarter annulus can be given by NURBS of degrees  $p_\xi = 1$  and  $p_\eta = 2$ , built upon the two knot vectors:

$$\Sigma_0 = \{0, 0, 1, 1\} \quad \text{and} \quad \Pi_0 = \{0, 0, 0, 1, 1, 1\}, \quad (25)$$

and the 6 control points  $P_{ij}$ ,  $i = 1, 2$  and  $j = 1, 2, 3$ , given in Table B1 (see the Appendix). In what follows, we will refer to this parameterization as  $Q_0$ .

In this section, together with  $Q_0$ , we will consider four 4-element parameterizations of the quarter annulus. Three will be called “uniform”, denoted by letters  $A$ ,  $B$ , and  $D$ , and one will be called “nonuniform”, denoted by letter  $C$ . Note that the



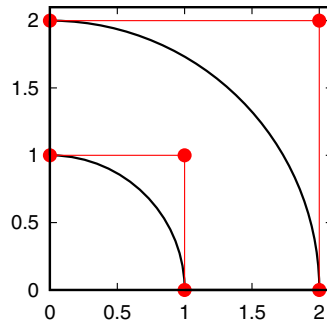


**FIGURE 5** Coarsest parameterization of a quarter annulus  $Q_0$ : 1 element and 6 control points [Colour figure can be viewed at wileyonlinelibrary.com]

parameterization  $D$  is obtained from the parameterization  $A$  by setting all the weights to 1. It does not exactly represent the quarter annulus, and it will only be used for solution approximation.

- The “uniform” parameterizations are obtained by performing the standard operation of knot insertion on knot vectors  $\Sigma_0$  and  $\Pi_0$  to calculate the positions  $P_{ij}$  and the weights  $w_{ij}$  of the corresponding control points. We add knot value  $s$  in the  $\xi$  direction and knot value  $t$  in the  $\eta$  direction. Then, the geometry is given by

$$\Sigma_1 = \{0, 0, s, 1, 1\} \quad \text{and} \quad \Pi_1 = \{0, 0, 0, t, 1, 1, 1\}. \tag{26}$$

- The “nonuniform” parameterization is obtained by adding two knot values  $s$  and  $t$  to the knot vectors  $\Sigma_0$  and  $\Pi_0$ , analogously to Equation (26) but arbitrarily choosing the weights and the position of two inner control points:  $P_{2,2}$  and  $P_{2,3}$ .
- The control points  $P_{ij}$  and the corresponding weights  $w_{ij}$  for parameterizations  $A_1, B_1, C_1$ , and  $D_1$  are listed in Tables B2, B3, B4, and B5, respectively.
- The higher-order parameterizations  $A_2, B_2, C_2$ , and  $D_2$  are obtained by standard degree elevation (by one in both directions) of parameterizations  $A_1, B_1, C_1$ , and  $D_1$ , respectively. Thereafter, the degrees of the parameterizations  $A_2, B_2, C_2$ , and  $D_2$  will be given by  $p_\xi = 2$  and  $p_\eta = 3$ .
- Moreover, for a special case, we will also consider a parameterization  $D_0$ , where  $p_\xi = 1$  and  $p_\eta = 1$ , and which is obtained by degree reduction of parameterization  $D_1$ .

The parameterizations  $A_1$  and  $C_1$  are shown in Figures 6 and 7. Note that, in this case, the term “elements” refers to the elements in the geometry parameterization (defined by two nonvanishing knot spans in each direction).

As discussed in the following section, a total of 19 patch tests for each of the problems of Section 3.1 (in 2 dimensions) are studied. Therefore, for better readability and classification, we introduce the following notation. We will denote a patch test by  $T_{G_i, S_j}^\ell$ , where the superscript  $\ell = 0, 1, \dots, 5$ , denotes the patch test case,  $G_i$  denotes the basis for geometry parameterization, and  $S_j$  denotes the basis for solution approximation. The bases  $G_i$  and  $S_j$  are chosen from the bases set given in Table 1 and their degree elevated/reduced versions.

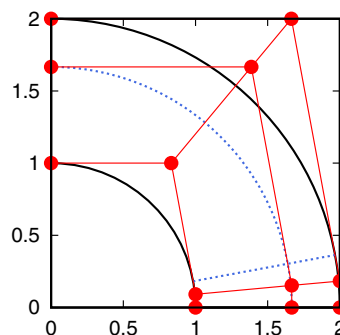


**FIGURE 6** Uniform parameterization  $A_1$ : elements and control points [Colour figure can be viewed at wileyonlinelibrary.com]

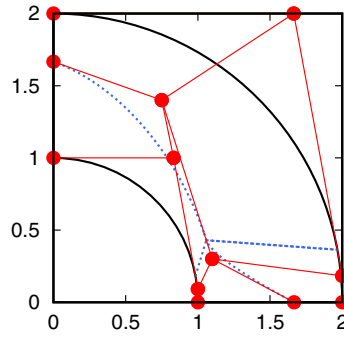


**FIGURE 7** Nonuniform parameterization  $C_1$ : elements and control points [Colour figure can be viewed at [wileyonlinelibrary.com](http://wileyonlinelibrary.com)]

**TABLE 1** Various parameterizations

	$p_\xi$	$p_\eta$	$s$	$t$	$P_{ij} \& w_{ij}$
$A_1$	1	2	2/3	1/8	Table B2
$B_1$	1	2	0.17	0.81	Table B3
$C_1$	1	2	2/3	1/8	Table B4
$D_1$	1	2	2/3	1/8	Table B5

### 3.3 | Results and discussion of patch tests

We start the series of patch tests by choosing the coarsest parameterization of the quarter annulus, ie,  $Q_0$ , paired with different bases for the solution.

The results of the first patch test are denoted by  $T^0$  in Table 2. Note that all the combinations of basis functions fall within the isoparametric or subparametric finite element concept. However, the first 2 combinations pass the test, whereas the other 2 fail. Therefore, in order to understand the connection between the geometry and the solution bases, which leads to either passing or failing the patch test, we introduce the following examples, investigating other choices of the geometry parameterization and solution approximation.

In the next patch test, denoted by  $T^1$  in Table 2, we demonstrate the performance of uniform parameterizations  $A_1$  and  $A_2$ . All 3 combinations pass the patch test. Note that the test  $T^1_{A_1, A_1}$  is a standard IGA patch test within isoparametric concept, which can exactly represent a constant/linear solution on any basis, which preserves the partition of unity. To understand the relation between geometry representation and solution approximation, we substitute the geometry parameterization

$$\begin{pmatrix} x \\ y \end{pmatrix} = \sum_{ij} \begin{pmatrix} P_{ij}^{A_1, x} \\ P_{ij}^{A_1, y} \end{pmatrix} \times \{\text{Basis of } A_1\} \quad (27)$$

and the solution approximation

$$u = \sum_{ij} u_{ij} \times \{\text{Basis of } A_1\} \quad (28)$$

into the solution

$$u = 1 + x + y \quad (29)$$

and obtain the solution control variables as

$$u_{ij} = 1 + P_{ij}^{A_1, x} + P_{ij}^{A_1, y}. \quad (30)$$

Now, recall the following fundamental property of the degree elevation algorithm (see algorithm 5.9 in the work of Piegl and Tiller<sup>51(p206)</sup>), which preserves the exactness of the geometry representation,

$$\begin{aligned} \begin{pmatrix} x \\ y \end{pmatrix} &= \sum_{ij} \begin{pmatrix} P_{ij}^{A_1, x} \\ P_{ij}^{A_1, y} \end{pmatrix} \times \{\text{Basis of } A_1\} \\ &= \sum_{ij} \begin{pmatrix} P_{ij}^{A_2, x} \\ P_{ij}^{A_2, y} \end{pmatrix} \times \{\text{Basis of } A_2\}. \end{aligned} \quad (31)$$

**TABLE 2** Results of various patch tests in terms of  $\|e\|_{L^2(\Omega)}$ . We say that the patch test is passed if  $\|e\|_{L^2(\Omega)} < 10^{-13}$  and fails if otherwise

$T_{G_i, S_j}^e$	Laplace Equation (22)	Elasticity Equation (24)
$T_{Q_0, A_1}^0$	1.3815e-15	3.0871e-14
$T_{Q_0, A_2}^0$	5.2147e-15	1.7986e-14
$T_{Q_0, C_1}^0$	0.0182	0.0050
$T_{Q_0, C_2}^0$	0.0023	0.0012
$T_{A_1, A_1}^1$	1.0023e-15	1.1675e-14
$T_{A_1, A_2}^1$	4.3958e-14	1.2547e-14
$T_{A_2, A_1}^1$	1.4059e-15	1.5525e-15
$T_{B_1, A_1}^2$	1.4755e-15	2.9941e-15
$T_{B_1, A_2}^2$	2.1639e-15	1.2118e-14
$T_{B_2, A_1}^2$	1.0144e-15	5.4590e-15
$T_{C_1, C_1}^3$	1.1061e-15	1.6439e-14
$T_{C_1, C_2}^3$	1.8263e-15	2.8737e-15
$T_{C_2, C_1}^3$	1.2062e-15	5.6517e-14
$T_{C_1, A_1}^4$	0.0203	0.0085
$T_{C_1, A_2}^4$	0.0016	0.0009
$T_{C_2, A_1}^4$	0.0203	0.0085
$T_{A_1, D_1}^5$	0.0188	0.0214
$T_{A_1, D_2}^5$	0.0121	0.0039
$T_{A_1, D_0}^5$	0.5418	0.1411

The test  $T_{A_1, A_2}^1$  can be viewed analogous to the FEA subparametric approach (the degree of the solution approximation is higher than the degree of the geometry). If the solution is approximated by

$$u = \sum_{ij} u_{ij} \times \{\text{Basis of } A_2\}, \quad (32)$$

then, using (31), the corresponding control variables can be found as

$$u_{ij} = 1 + P_{ij}^{A_2, x} + P_{ij}^{A_2, y}. \quad (33)$$

The test  $T_{A_2, A_1}^1$  can be viewed analogous to the FEA superparametric approach (the degree of the solution approximation is lower than the degree of the geometry). However, the essential difference is that the geometry degree was artificially lifted from  $A_1$  to  $A_2$ . Since using (31) in (29) yields the solution given by (30), this means that both the bases  $A_1$  and  $A_2$ , as well as any two parameterizations with the same property, yield identical solutions for the solution control variables (within the numerical tolerance).

For the second patch test, denoted by  $T^2$  in Table 2, we consider the situation when we have two uniform but different parameterizations of the domain, and one of them is used to parameterize the geometry and the second one is used as a basis to approximate the unknown solution. All the three combinations pass the test. Note that, in this test, we used the same basis for the solution approximation as in the test 1 but a different geometry parameterization  $B_1$  (instead of  $A_1$ ). However, both parameterizations,  $A_1$  and  $B_1$ , were obtained from the coarsest parameterization  $Q_0$  of the quarter

annulus. According to the property of the knot insertion algorithm (see algorithm 5.3 in the work of Piegl and Tiller<sup>51(p155)</sup>), this gives

$$\begin{aligned} \begin{pmatrix} x \\ y \end{pmatrix} &= \sum_{ij} \begin{pmatrix} P_{ij}^{A_1, x} \\ P_{ij}^{A_1, y} \end{pmatrix} \times \{\text{Basis of } A_1\} \\ &= \sum_{ij} \begin{pmatrix} P_{ij}^{B_1, x} \\ P_{ij}^{B_1, y} \end{pmatrix} \times \{\text{Basis of } B_1\}. \end{aligned} \quad (34)$$

Because of the property (34), geometry parameterizations  $A_1$  and  $B_1$  (as well as their higher-degree versions  $A_2$  and  $B_2$  or any other two parameterizations with the same property) analytically yield the results for the solution control variables in  $T^2$  to be identical (within the numerical tolerance) to the solution control variables in  $T^1$ , which is given by Equation (30) (or for higher degree by Equation (33)). Note that the same property holds between bases  $Q_0$  and  $A_1$  in the test  $T^0$ , which implies that the solution in  $T_{Q_0, A_1}^0$  is expressed by Equation (30), and by adding the property of degree elevation Equation (31), we can conclude that the solution in  $T_{Q_0, A_2}^0$  is given by Equation (33).

In the third patch test, denoted by  $T^3$  in Table 2, we investigate the performance of nonuniform parameterization. The results of the third patch test show that all the three combinations pass the test. In fact, in this test, only the degree elevation algorithm (from  $C_1$  to  $C_2$ ) is used, which makes it fully analogous to  $T^1$ , albeit with a nonuniform parameterization.

In tests  $T^1$ ,  $T^2$ , and  $T^3$ , the bases of solution and geometry were related, either both the bases were obtained from the geometry parameterization  $Q^0$  (as in tests  $T^1$  and  $T^2$ ) or the solution basis was obtained from the geometry basis (as in test  $T^3$ ). The idea of the fourth patch test, denoted by  $T^4$  in Table 2, is to show the combinations of the geometry parameterizations and solution approximations, which will fail to produce the linear solution. For this purpose, we use the same approximation bases  $A_1$  and  $A_2$  for the solution, as in  $T^1$  and  $T^2$ , but combined with the nonuniform geometry parameterization  $C_1$  and  $C_2$ . As it is seen from Table 2, this test fails for all the combinations. Due to the fact that  $C_1$  was not derived from the coarsest parameterization  $Q_0$  of the quarter annulus, the property analogous to (34), between  $A_1$  and  $C_1$ , does not hold.

In the fifth patch test, denoted by  $T^5$  in Table 2, the conditions (31) and (34) between the geometry parameterization and the solution approximation do not hold, and therefore, as expected, all combinations of  $T^5$  fail. However, this case is important for practical applications, and the suggested bases combinations will be used later in the numerical examples. We use the NURBS basis  $A_1$  for geometry parameterization and the B-spline basis  $D_i$ ,  $i = \{0, 1, 2\}$  for solution approximation. Two important features of  $T^5$  are the following.

- The superparametric case is different from what is considered in the previous patch tests because, instead of artificially lifting the degree of the geometry parameterization, we kept the minimum required order of the geometry basis, and reduced the degree of the solution approximation.
- In all previous patch tests, the basis used for the solution approximation could also be used to exactly represent the geometry. However, in  $T^5$ , the B-spline basis, which is used for the solution, cannot exactly represent the geometry.

**Conclusion:** The **sufficient condition** for the patch test to pass consists in the requirement for the geometry and field bases to be equivalent, up to operations of degree elevation and/or knot insertion or, in other words, to have a common “parent basis”, from which they were obtained by operations of degree elevation and/or knot insertion.

## 4 | NUMERICAL RESULTS

In this section, we present convergence results of various basis choices for the geometry and the numerical solution. We consider 2 classes of problems, namely, the Laplace/Poisson problem and the problem of linear elasticity.

In Section 4.1, we first present the problem data of all the numerical examples, ie, analytic solution, boundary data, forcing function, geometry parameterization, and the basis for numerical solution. In Section 4.2, we discuss the convergence results of these examples. In Section 4.3, we comment on the relation of the convergence results with patch tests, and relate with the asymptotic theoretical convergence. Finally, in Section 4.4, we propose a new naming convention for the choices of basis orders with respect to the isogeometric paradigm.

### 4.1 | Description of various examples

**Example 1.** Consider the Laplace problem in the quarter annulus domain of Figure 4, together with the exact solution

$$u(r, \theta) = r^{-3} \cos(3\theta), \tag{35}$$

which is prescribed as Dirichlet boundary condition on all boundaries. This geometry is exactly represented by the NURBS basis  $\mathcal{N}_{1,2}$ . The convergence study cases are based on the choices of geometry and solution bases, which are used in the patch tests in Section 3 (see Table 2).

**Example 2.** Consider the problem of a thick-walled cylinder under a uniform internal and external pressure, as shown in Figure 8. Instead of the full problem, a quarter annulus is considered with the symmetry boundary conditions along  $x = 0$  and  $y = 0$ , and the following boundary conditions on the inner and outer boundary of the cylinder are imposed:

$$\sigma_r(r_1) = -p_1, \quad \sigma_r(r_2) = -p_2. \tag{36}$$

The solution of this problem in polar coordinates, under plane strain assumption, is given by

$$\sigma_r(r) = s_1 r^{-2} + s_2, \quad \sigma_\theta(r) = -s_1 r^{-2} + s_2, \quad u_r(r) = s_3 (-s_1 r^{-1} + s_2 r), \tag{37}$$

where  $s_1 = \frac{r_1^2 r_2^2 (p_2 - p_1)}{r_2^2 - r_1^2}$ ,  $s_2 = (1 - 2\nu) \frac{r_1^2 p_1 - r_2^2 p_2}{r_2^2 - r_1^2}$ , and  $s_3 = \frac{1 + \nu}{E}$ . The numerical tests were performed on the same choices of the combination of geometry-solution bases, as in Example 1 for Laplace equation (see also Table 2).

**Example 3.** Consider the Laplace problem in a wedge geometry (see Figure 9), together with the exact solution

$$u = \log((x + 0.1)^2 + (y + 0.1)^2), \tag{38}$$

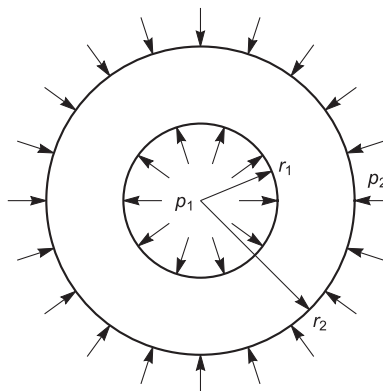


**FIGURE 8** Thick-walled pressurized cylinder, Example 2

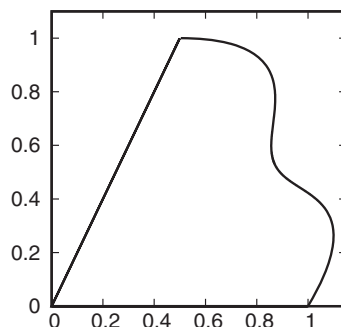


**FIGURE 9** Wedge geometry, Example 3

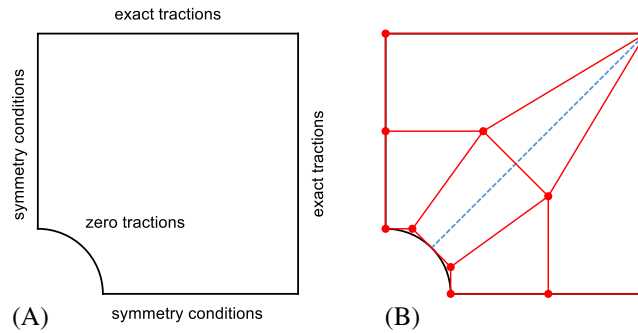


**FIGURE 10** Geometry and parameterization, Example 4. A, Quarter of the plate with a hole, subjected to the boundary conditions given by Equation (39); B, Control net and element boundaries in the plate parameterization [Colour figure can be viewed at [wileyonlinelibrary.com](http://wileyonlinelibrary.com)]

which is prescribed as a Dirichlet boundary condition on all boundaries. The choice of this geometry is motivated by the observation in the superparametric case of Example 1. As opposed to the patch test cases, where the degree for geometry representation was artificially lifted, the geometry in this case is given by a tensor product of NURBS of degrees  $p_\xi = 1$  and  $p_\eta = 4$ . In this example, we focus on subparametric and superparametric solution approximations. As the geometry parameterization is fixed (we denote the corresponding NURBS basis by  $\mathcal{N}_{1,4}$ ), to ease with the naming, we use the notation of paired bases as  $(\mathcal{N}_{1,4}, S_{k,l})$ , where  $S_{k,l}$  denotes the basis for solution approximation ( $S = \mathcal{N}$  for NURBS as well as  $S = \mathcal{B}$  for B-splines),  $k$  denotes the degree in the  $\xi$  direction, and  $l$  denotes the degree in the  $\eta$  direction. For subparametric solution approximations, we only elevate the degree in the  $\xi$  direction, ie,  $k = 2$ , and for superparametric solution approximations, we only consider degree reduction in the  $\eta$  direction, ie,  $1 \leq l \leq 3$ .

**Example 4.** Consider a typical problem of a plate weakened by a circular hole of radius  $a$  and subject to remote tension  $T$  in the  $x$  direction. Only a quarter of a plate (of a finite size  $L = 4a$ ), as shown in Figure 10A, is modeled with the symmetry boundary conditions along  $x = 0$  and  $y = 0$ , and analytical tractions are prescribed on the rest of the boundary according to the following solution:

$$\begin{aligned}
 \sigma_{xx}(r, \theta) &= T - T \frac{a^2}{r^2} \left( \frac{3}{2} \cos 2\theta + \cos 4\theta \right) + T \frac{3a^4}{2r^4} \cos 4\theta, \\
 \sigma_{yy}(r, \theta) &= -T \frac{a^2}{r^2} \left( \frac{1}{2} \cos 2\theta - \cos 4\theta \right) - T \frac{3a^4}{2r^4} \cos 4\theta, \\
 \sigma_{xy}(r, \theta) &= -T \frac{a^2}{r^2} \left( \frac{1}{2} \sin 2\theta + \sin 4\theta \right) + T \frac{3a^4}{2r^4} \sin 4\theta, \\
 u_x(r, \theta) &= \alpha_0 \left( \frac{4r}{a} (1 - \nu) \cos \theta + \frac{2a}{r} (4(1 - \nu) \cos \theta + \cos 3\theta) - \frac{2a^3}{r^3} \cos 3\theta \right), \\
 u_y(r, \theta) &= \alpha_0 \left( \frac{r}{a} (-4\nu) \sin \theta + \frac{2a}{r} (-2(1 - 2\nu) \sin \theta + \sin 3\theta) - \frac{2a^3}{r^3} \sin 3\theta \right),
 \end{aligned} \tag{39}$$

where  $\alpha_0 = (1 + \nu)Ta/(4E)$ . In all study cases for this problem, the geometry is parameterized by a basis of second order with the following knot vectors:

$$\Sigma = \{0, 0, 0, 1, 1, 1\}, \quad \Pi = \{0, 0, 0, 0.5, 1, 1, 1\}. \tag{40}$$

The corresponding control points are listed in Table B6. The parameterization consists of two elements (see Figure 10B) and remains unchanged during the solution refinement process (denoted by  $\mathcal{N}_{2,2}$ ). Following the notation of paired bases introduced in Example 3, we consider the following choices for the solution approximation basis:  $(\mathcal{N}_{2,2}, \mathcal{N}_{2,2})$ ,  $(\mathcal{N}_{2,2}, \mathcal{N}_{3,3})$ ,  $(\mathcal{N}_{2,2}, \mathcal{B}_{2,2})$ , and  $(\mathcal{N}_{2,2}, \mathcal{B}_{3,3})$ . Note that B-spline basis  $\mathcal{B}_{2,2}$  is built on knot vectors (40). We also consider another geometry parameterization, which is built on the knot vectors (40), with the boundary control points as listed in Table B6, but the weights of two inner points being changed to  $w_{2,2} = w_{2,3} = 0.9$ . This parameterization will be denoted by  $\tilde{\mathcal{N}}_{2,2}$ . Thereafter, we consider two more choices for the solution approximation basis:  $(\mathcal{N}_{2,2}, \tilde{\mathcal{N}}_{2,2})$ , and  $(\mathcal{N}_{2,2}, \tilde{\mathcal{N}}_{3,3})$ .

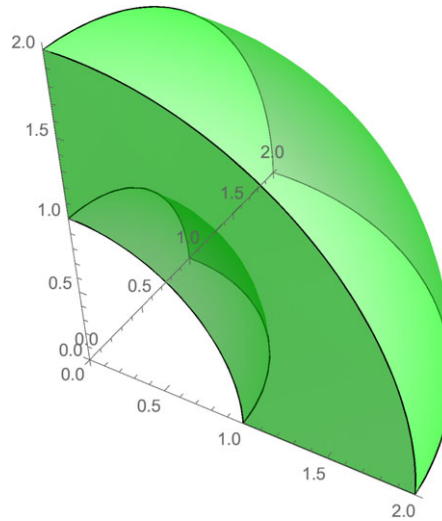


**FIGURE 11** One-eighth of a sphere, Example 5 [Colour figure can be viewed at wileyonlinelibrary.com]

**Example 5.** Consider a thick-walled sphere geometry with inner radius  $r_1$  and outer radius  $r_2$  (one-eighth of a hollow sphere for symmetry boundary conditions) (see Figure 11). The coarsest NURBS parameterization of this geometry can be given by degrees  $p_\xi = 1, p_\eta = 2$ , and  $p_\zeta = 2$ , built upon the knot vectors

$$\Sigma = \{0, 0, 1, 1\}, \quad \Pi = \{0, 0, 0, 1, 1, 1\}, \quad Z = \{0, 0, 0, 1, 1, 1\}, \tag{41}$$

with the control points listed in Table B7. We will refer to this parameterization as  $Q_1$ . Using the notations introduced earlier, the basis for this parameterization will be denoted by  $\mathcal{N}_{1,2,2}$ . We also consider the following choices of the bases for solution approximation:  $\mathcal{N}_{1,2,2}, \mathcal{N}_{2,2,2}, \mathcal{B}_{1,2,2}, \mathcal{B}_{2,2,2}$ , and  $\mathcal{B}_{1,1,1}$ . Note that we use the uniform refinement of  $Q_1$  for these bases (similar to the case  $A_1$  of Section 3.2). In addition, the basis  $\mathcal{B}_{1,1,1}$  is built on the knot vectors

$$\Sigma = \{0, 0, 1, 1\}, \quad \Pi = \{0, 0, 1, 1\}, \quad Z = \{0, 0, 1, 1\}. \tag{42}$$

The problem in consideration is a well-known thick-walled pressurized sphere, ie, the hollow sphere subjected to the following boundary conditions (in spherical coordinates  $r, \theta, \phi$ ):

$$\sigma_{rr} = -p_1 \quad \text{at} \quad r = r_1, \quad \sigma_{rr} = -p_2 \quad \text{at} \quad r = r_2. \tag{43}$$

On the rest of the boundary, the symmetry conditions are prescribed. The analytical solution is given by

$$u_r(r) = (\alpha_1 r + \alpha_2 r^{-2}) / \alpha_3, \tag{44}$$

where  $\alpha_1 = 2(p_1 r_1^3 - p_2 r_2^3)(1 - 2\nu)$ ,  $\alpha_2 = (p_1 - p_2)(1 + \nu)r_1^3 r_2^3$ , and  $\alpha_3 = 2E(r_2^3 - r_1^3)$ .

**Example 6.** This example is to demonstrate the effectiveness of the proposed method by using the weak coupling of bases for geometry and simulation. The geometry is represented by NURBS, whereas the numerical solution is obtained using PHT-splines (see Appendix A for necessary details).

Consider again an annulus region in two dimensions (see Figure 4) described by a quadratic  $C^1$  NURBS surface with  $3 \times 3$  control points and following knot vectors on the parametric domain

$$\Sigma = [0, 0, 0, 1, 1, 1], \quad \Pi = [0, 0, 0, 1, 1, 1].$$

Consider the Poisson problem with homogeneous Dirichlet boundary conditions, and choose the source function such that the exact solution of the problem has the following form:

$$u(r, \theta) = (r - 1)(r - 2)\theta \left( \theta - \frac{\pi}{2} \right) \exp(-100(r \cos \theta - 1)^2), \tag{45}$$

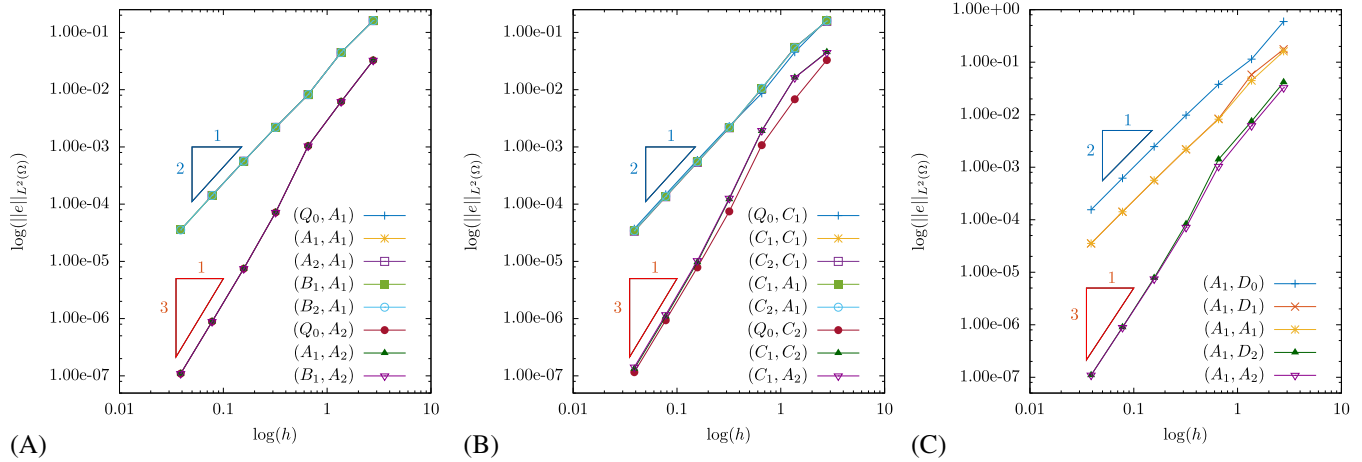


**FIGURE 12** Convergence study for Example 1. A, Geometry parameterizations  $Q_0, A_1, A_2, B_1,$  and  $B_2$  combined with solution bases  $A_1$  and  $A_2$ ; B, Geometry parameterizations  $C_1$  and  $C_2$  combined with solution bases  $C_1, C_2, A_1,$  and  $A_2$ ; C, B-splines solution bases:  $D_0, D_1,$  and  $D_2$  [Colour figure can be viewed at [wileyonlinelibrary.com](http://wileyonlinelibrary.com)]

where

$$r(x, y) = \sqrt{x^2 + y^2}, \quad \theta = \arctan(y/x).$$

## 4.2 | Convergence studies of various examples

### 4.2.1 | Example 1

The convergence rates in  $L^2$ -norm for all study cases are shown in Figures 12A, 12B, and 12C. The results are combined as follows.

In Figure 12A, we have collected 3 choices of geometry parameterization, namely the coarsest  $Q_0$ , and its variations  $A_1, A_2, B_1,$  and  $B_2$ . Since  $A_1, A_2, B_1,$  and  $B_2$  are equivalent to  $Q_0$  up to the knot insertion and degree elevation, the convergence results are identical, and the slope of the graph depends only on the lowest degree of the solution approximation (1 in the case of  $A_1$ , and 2 in the case of  $A_2$ ).

In Figure 12B, we show the results for the nonuniform geometry parameterizations  $C_1$  and  $C_2$  and the solution bases  $C_1, C_2, A_1,$  and  $A_2$ , in comparison with the coarsest geometry parameterization  $Q_0$  paired with the solution bases  $C_1$  and  $C_2$ . Despite the slight difference in the results associated with the choice of the geometry representation, all graphs exhibit the expected convergence rates, which is governed by the lowest degree of the solution approximation.

Finally, in Figure 12C, we included the results for the fifth case (represented by  $T^5$  in Table 2), characterized by the fact that the B-splines-based solution basis cannot represent the geometry exactly. The pairs  $A_1-D_0, A_1-D_1,$  and  $A_1-D_2$  are shown in comparison with  $A_1-A_1$  and  $A_1-A_2$ . Despite the difference in weights of the basis functions between  $A_1-A_1$  and  $A_1-D_1$  (as well as between  $A_1-D_2$  and  $A_1-A_2$ ), the difference in the results is very minor. This makes us conclude that, though the B-splines solution basis fails the patch test, it is nevertheless a suitable basis for the analysis. Moreover, the case  $A_1-D_0$ , which can be regarded as truly superparametric in the FEA context, also exhibits the expected convergence rate. This surprising result counters the established practice of FEM, where a superparametric approach is not recommended.<sup>52</sup>

### 4.2.2 | Example 2

The results of numerical simulations are organized in 3 plots: Figure 13A, 13B, and 13C. The obtained numerical solutions exhibit a similar pattern as that observed in Example 1, ie, the graphs show that the convergence rate of the solution is defined by the lowest degree in the solution basis, independent of the (exact) geometry parameterization.

### 4.2.3 | Example 3

In Figure 14, we present the results for the following 7 cases:  $(\mathcal{N}_{1,4}, \mathcal{N}_{1,4}), (\mathcal{N}_{1,4}, \mathcal{B}_{1,4}), (\mathcal{N}_{1,4}, \mathcal{N}_{2,4}), (\mathcal{N}_{1,4}, \mathcal{B}_{2,4}), (\mathcal{N}_{1,4}, \mathcal{B}_{1,1}), (\mathcal{N}_{1,4}, \mathcal{B}_{1,2}),$  and  $(\mathcal{N}_{1,4}, \mathcal{B}_{1,3})$ . As we can observe from the numerical studies presented in Figure 14, together with the exact



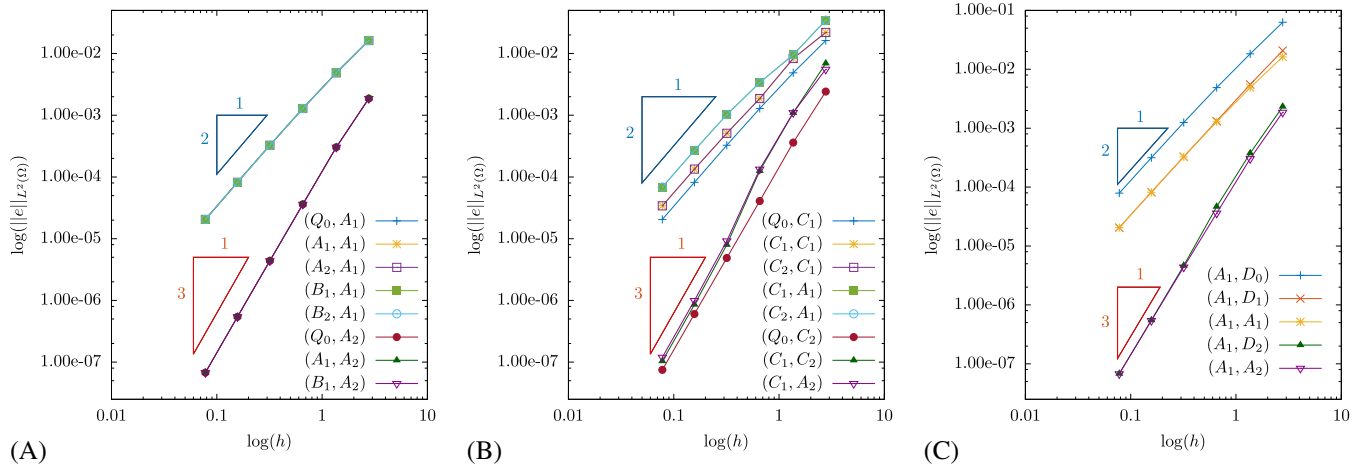


**FIGURE 13** Convergence study for Example 2. A, Geometry parameterizations  $Q_0, A_1, A_2, B_1,$  and  $B_2$  combined with solution bases  $A_1$  and  $A_2$ ; B, Geometry parameterizations  $C_1$  and  $C_2$  combined with solution bases  $C_1, C_2, A_1,$  and  $A_2$ ; C, B-splines solution bases:  $D_0, D_1,$  and  $D_2$  [Colour figure can be viewed at wileyonlinelibrary.com]

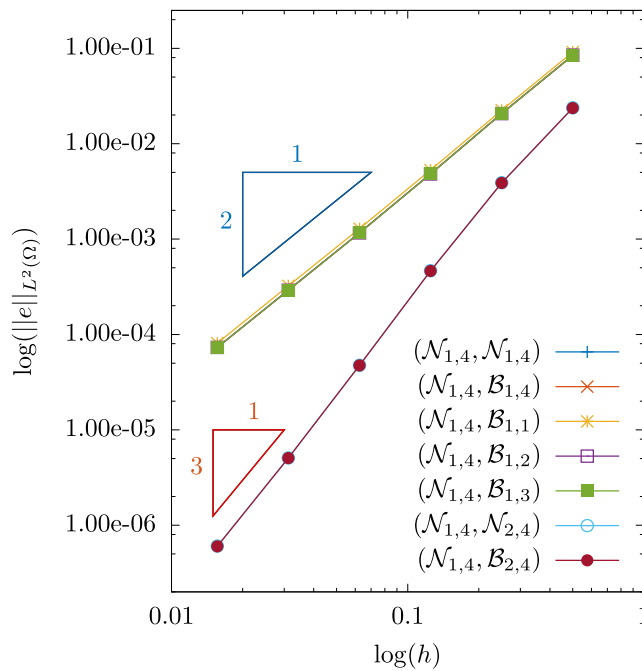


**FIGURE 14** Convergence study for Example 3 [Colour figure can be viewed at wileyonlinelibrary.com]

representation of the geometry, the convergence rate depends only on the lowest degree in the solution approximation, and the results for NURBS and B-spline solution bases are almost identical.

**4.2.4 | Example 4**

The results of these study cases are shown in Figure 15, where it can be seen that the convergence rate for all choices of the solution basis depends only on the order of the solution basis, and for the bases of the same order, the results for different basis functions are almost identical.

**4.2.5 | Example 5**

The numerical results are shown in Figure 16, where it can again be seen that the convergence rate in all the 5 cases depends only on the approximation basis for the numerical solution.

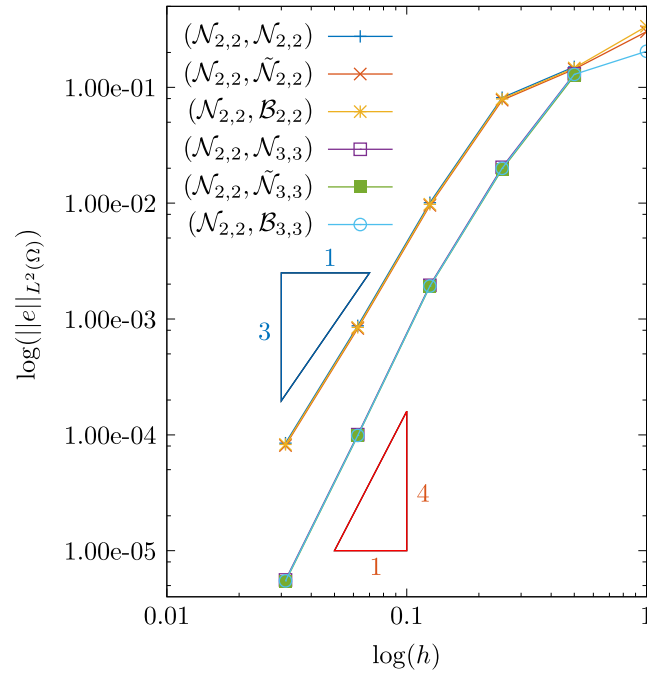


FIGURE 15 Convergence study for Example 4 [Colour figure can be viewed at wileyonlinelibrary.com]

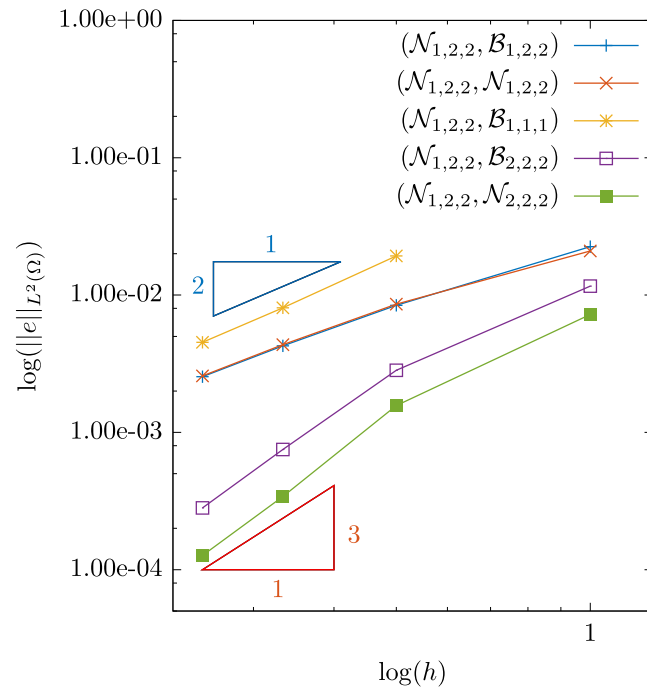
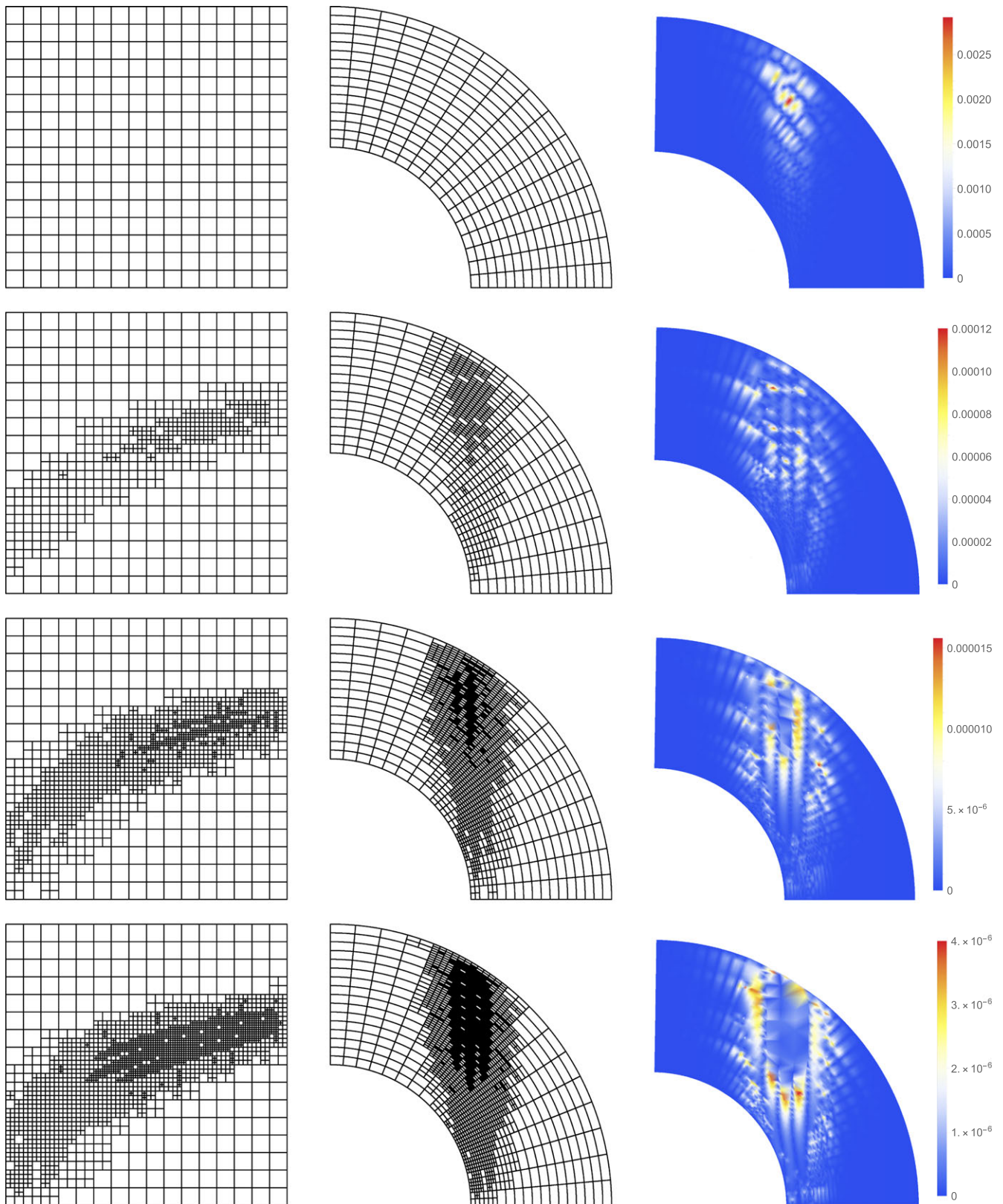


FIGURE 16 Convergence study for Example 5 [Colour figure can be viewed at wileyonlinelibrary.com]

### 4.2.6 | Example 6

In Figure 17, we show the results during local refinement operations. From the first row to the fourth row, we show the T-mesh on the parametric domain (left), the mesh on the physical domain (middle), and the corresponding exact error color map on the physical domain (right). In Figure 18, we present the convergence behavior of 4 choices of geometry and simulation bases, which are as follows:

- (1) IGA with cubic NURBS (for the geometry as well as the numerical solution). Note that a NURBS of  $p_\xi = 1$  and  $p_\eta = 2$  is sufficient for this geometry. However, to have a fair comparison with the remaining studies, we



**FIGURE 17** Example 6. The Geometry-Independent Field approximation approach for a problem with exact solution having sharp peaks. The geometry representation is based on the coarsest nonuniform rational B-splines with  $p_\xi = 1$  and  $p_\eta = 2$ , and the numerical solution is based on  $C^1$  PHT-splines, the latter enabling local refinement. From the first row to the fourth row, we show the T-mesh in the parametric domain (left), the mesh on the physical domain (middle), and the corresponding error color map on the physical domain during local refinement operations (right)

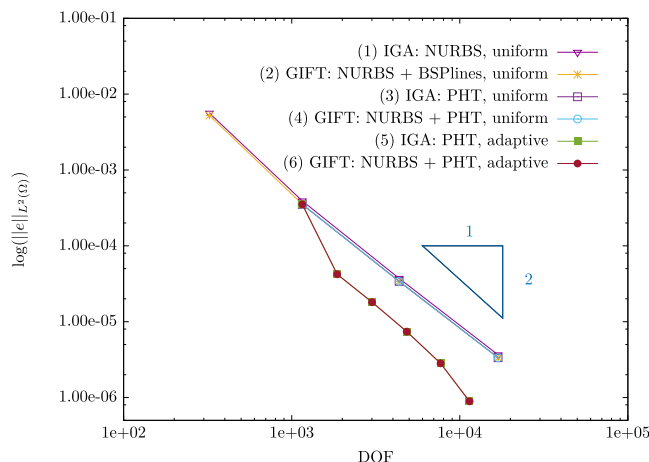


**FIGURE 18** Convergence study for Example 6. The isogeometric analysis (IGA) method with cubic NURBS, IGA method with cubic PHT-splines, Geometry-Independent Field approximation (GIFT) method with cubic B-splines, and GIFT method with cubic PHT-splines (as in Figure 17). NURBS, nonuniform rational B-splines [Colour figure can be viewed at [wileyonlinelibrary.com](http://wileyonlinelibrary.com)]

elevate the degree to  $p_\xi = p_\eta = 3$ , while maintaining the exact geometry representation. In this example, during the  $h$ -refinement we inserted each knot twice to have the  $C^1$ -continuous basis for a fair comparison with the PHT splines.

- (2) GIFT with NURBS of  $p_\xi = 1$  and  $p_\eta = 2$  for the geometry, and cubic B-splines for the numerical solution. In this example, during the  $h$ -refinement of the solution basis, we inserted each knot twice to have the  $C^1$ -continuous basis. The NURBS geometry was kept unchanged during the solution refinement process.
- (3, 5) IGA with cubic PHT-splines (for the geometry as well as the numerical solution). Note that, in this case, the computational geometry is only an approximate (not exact as in IGA with cubic NURBS). In this example, both, uniform (3) and adaptive (5), refinements were performed.
- (4, 6) GIFT with NURBS of  $p_\xi = 1$  and  $p_\eta = 2$  for the geometry and cubic PHT-splines for the numerical solution. In this example, both, uniform (4) and adaptive (6), refinements of the PHT-splines basis were also performed.

From the convergence plots, we conclude the following.

1. Analogous to the results observed in earlier studies, IGA with cubic NURBS (1), GIFT with cubic B-splines (2), and both, IGA (3) and GIFT (4) with cubic uniformly refined PHT-splines, exhibit same convergence rate. This is because all three solution bases are of the same degree. Note that convergence curves (1), (2), (3), (4) are quasi-identical, meaning that the error is influenced by the solution basis significantly more than by the choice of the domain parameterization.
2. Owing to the local adaptive refinement of the solution basis, both the cases of PHT-splines (IGA as well as the proposed GIFT, ie, (5 and 6)) exhibit slight improvement in the convergence rate of the overall error than the same examples with uniform refinement of the PHT-spline basis (3 and 4).
3. The comparison of IGA with PHT-splines (3, 5) and GIFT with PHT-splines (4, 6) solution highlights an important difference. The advantage of the exact geometry representation in the latter case over an approximate geometry in the former case is very minor. This is due to the fact that the geometry of the computational domain is simple, and can be accurately approximated with the PHT-splines of third degree (geometry approximation error is below the discretization error). However, in realistic industrial problems with complex domains, this advantage will become more pronounced. In comparison with standard IGA with PHT splines, employing the exact coarse NURBS geometry parameterization in GIFT (together with PHT-splines solution) brings two distinct advantages.
  - It eliminates the need to communicate with the original CAD model at each step of the solution refinement process, and the approximation of the boundaries.
  - It also eliminates the need to refine the original coarse geometry, as well as to store and process the refined data, which can lead to significant computational savings for big problems.

### 4.3 | Discussion on numerical results

The results of Section 3 indicate that a **sufficient condition** for the combination of the geometry and the solution bases to pass the **classical patch test** is the requirement that these two bases are equivalent up to the degree elevation (31) and/or knot insertion operations (34), which ensure the preservation of the geometry exactness. However, we see from the numerical results in Section 4.2 that, despite failing the classical patch test, all cases presented in Table 2 exhibit optimal-order convergence. This includes the bases derived from the geometry parameterization  $A$  and  $B$ , the nonuniform parameterization  $C$ , and the B-spline basis  $D$  (which cannot represent the geometry exactly). This is not surprising, however. Thanks to lemma 3.4-3.5 and theorem 3.1-3.2 with a suitable projector  $\Pi_{V_h}$  in the work of Bazilevs et al,<sup>53</sup> the optimal-order global error estimates hold for every function  $v \in H^l(\Omega)$ . The effect of geometry mapping is included in the definition of the element size  $h_K = \|\nabla F\|_{L^\infty(Q)} h_Q$ , where  $F$  is the geometry mapping,  $Q$  is the element in the parametric domain, and  $h_Q$  is the element size in the parametric domain. Moreover, the constant  $C_{\text{shape}}$  appearing in lemma 3.4-3.5 and theorem 3.1-3.2 in the work of Bazilevs et al<sup>53</sup> depends only on the weight function  $w$  and its reciprocal  $1/w$  on  $\tilde{Q}$ , where  $\tilde{Q}$  is the support extension of  $Q$ , and is uniformly bounded with respect to the mesh size. This observation is in alignment with the work of Stummel<sup>50</sup> that the classical patch test is neither necessary nor sufficient for convergence. Therefore, together with exact geometric representation, a suitable basis (derived from or related to geometry parameterization) can be used for optimal-order convergence. For a quick comparison, in Table 3, we recall all the cases studied in this paper.

Nevertheless, it is important to exercise caution while devising a basis for the numerical solution. In all our numerical examples 1 to 5, the solution basis was constructed on the basis of the same knot vectors as the geometry parameterization. This assures the continuity of the geometry parameterization within solution elements. For Example 4, we now consider the coarsest basis consisting of B-splines of degree  $2 \times 2$  defined on the knot vectors (denoted by  $\tilde{B}_{2,2}$ )

$$\Sigma = \{0, 0, 0, 1, 1, 1\}, \quad \Pi = \{0, 0, 0, 0.166667, 1, 1, 1\}. \quad (46)$$

In this case, the singular point ( $x = L, y = L$ ) is inside an element of any mesh for the numerical solution. As it can be seen from Figure 19, the solution does not exhibit the expected convergence rate. Though a thorough mathematical derivation of the presented approach is a subject of future research, we recommend to avoid those combination of geometry-solution bases where the continuity of the geometry parameterization is violated in the solution elements.

**TABLE 3** Summary of patch tests and optimal convergence. See Section 3.2 for the notations  $Q, A, B, C$ , and  $D$ . For the degree parity, we used the naming convention with respect to the geometry, see Table 4

Geometry Parameterization	Solution Basis	Degree Parity	Patch Test	Optimal Convergence
$Q_0$	$A_1$	Isogeometric	✓	✓
$Q_0$	$A_2$	Supergeometric	✓	✓
$Q_0$	$C_1$	Isogeometric	×	✓
$Q_0$	$C_2$	Supergeometric	×	✓
$A_1$	$A_1$	Isogeometric	✓	✓
$A_1$	$A_2$	Supergeometric	✓	✓
$A_2$	$A_1$	Subgeometric	✓	✓
$B_1$	$A_1$	Isogeometric	✓	✓
$B_1$	$A_2$	Supergeometric	✓	✓
$B_2$	$A_1$	Subgeometric	✓	✓
$C_1$	$C_1$	Isogeometric	✓	✓
$C_1$	$C_2$	Supergeometric	✓	✓
$C_2$	$C_1$	Subgeometric	✓	✓
$C_1$	$A_1$	Isogeometric	×	✓
$C_1$	$A_2$	Supergeometric	×	✓
$C_2$	$A_1$	Subgeometric	×	✓
$A_1$	$D_1$	Isogeometric	×	✓
$A_1$	$D_2$	Supergeometric	×	✓
$A_1$	$D_0$	Subgeometric	×	✓

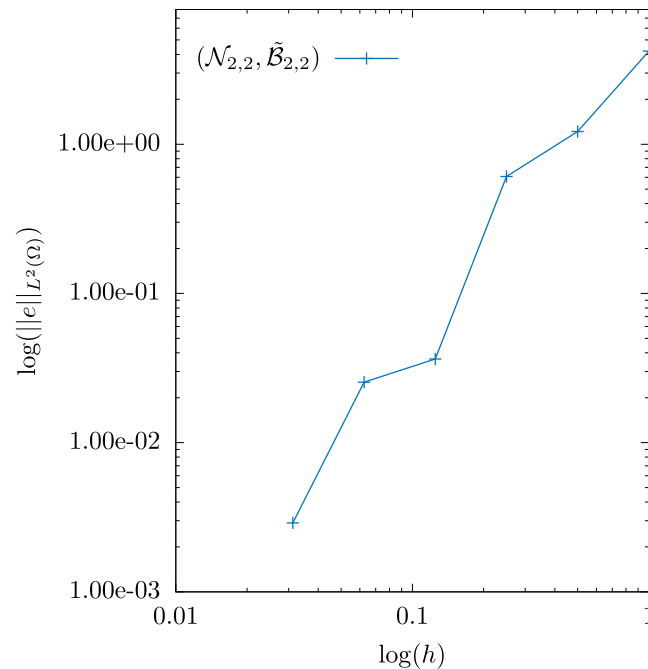


**FIGURE 19** Convergence study for Example 4 with knot vectors (46) [Colour figure can be viewed at wileyonlinelibrary.com]

**TABLE 4** Naming convention

	$p_u = p_g$	$p_u < p_g$	$p_u > p_g$
FEM	Isoparametric	Superparametric	Subparametric
GIFT	Isogeometric	Subgeometric	Supergeometric

Abbreviations: FEM, finite element method; GIFT, Geometry-Independent Field approximation.

#### 4.4 | Naming convention

Let  $p_u$  and  $p_g$  denote the degrees of the basis functions for the solution and the geometry, respectively. In the standard FE context, since the primary quantity of interest is the numerical solution, the naming convention is with respect to the parameter  $p_u$ . However, in IGA, the primary quantity is the geometry. Accordingly, for better readability, we propose the naming convention with respect to the parameter  $p_g$ , as presented in Table 4.

Note that, in standard FEM, the use of  $p_u < p_g$  (superparametric) case is not recommended.<sup>52(p172)</sup> However, the results presented in Example 3 show that, with exact geometry representation, superparametric approximations can also deliver optimal orders of convergence.

## 5 | CONCLUSIONS

We presented a method that relaxes the requirement for a tight coupling between the spaces for the representation of the geometry and the approximation of the field variables, but retains the main feature of isogeometric analysis, ie, the geometrical exactness and the ability to operate directly from geometry data.

In some cases, this relaxation for the choice of the boundary parameterization and the numerical solution leads to the failure of the classical patch test. We presented a detailed study of patch tests for various choices of geometry and solution bases, and demonstrated that even those choices, where the patch test is failed, nevertheless, yield optimal convergence.

We also showed that, for the same geometry parameterization, the choice of NURBS basis yields quasi-identical results to the choice of a polynomial basis (B-splines or PHT-splines). The latter brings a distinct advantage during the  $h$ -refinement since it eliminates the need to refine the weights in the solution basis. Moreover, the original NURBS

geometry is kept unchanged during the solution refinement, and therefore, the need to refine, process, and store the geometry data is also avoided.

We also showed that, to enable the local refinement, the NURBS geometry can be paired with a locally refinable solution basis, eg, PHT-splines. Local refinement is highly advantageous in capturing sharp gradients, and improving the convergence rate at a low computational cost.

## ACKNOWLEDGEMENTS

E. Atroshchenko and S.P.A. Bordas acknowledge the financial support of University of Luxembourg through its Computational Sciences research priority.

S.P.A. Bordas and S. Tomar thank the financial support of the European Research Council Starting Independent Research Grant (ERC Stg grant agreement 279578) entitled “Towards real time multiscale simulation of cutting in non-linear materials with applications to surgical simulation and computer guided surgery”, and the support of the Luxembourg National Research Funds INTER/FWO/15/10318764 and INTER/MOBILITY/14/8813215/CBM/Bordas.

G. Xu is supported by the National Nature Science Foundation of China under grants 61772163 and 61472111, Zhejiang Provincial Natural Science Foundation of China under grants LR16F020003 and LQ16F020005, and the Open Project Program of the State Key Lab of CAD&CG (A1703), Zhejiang University.

## ORCID

Elena Atroshchenko  <http://orcid.org/0000-0002-7871-9926>

Satyendra Tomar  <http://orcid.org/0000-0002-5706-5556>

Gang Xu  <http://orcid.org/0000-0003-3557-9529>

Stéphane P.A. Bordas  <https://orcid.org/0000-0001-8634-7002>

## REFERENCES

- Hughes T, Cottrell J, Bazilevs Y. Isogeometric analysis: CAD, finite elements, NURBS, exact geometry and mesh refinement. *Comput Meth Appl Mech Eng*. 2005;194(39-41):4135-4195.
- Reali A. An isogeometric analysis approach for the study of structural vibrations. *J Earthquake Eng*. 2006;10(1):1-30.
- Bazilevs Y, Calo VM, Hughes TJR, Zhang Y. Isogeometric fluid-structure interaction: theory, algorithms, and computations. *Comput Mech*. 2008;43(1):3-37.
- Benson D, Bazilevs Y, Hsu M, Hughes T. Isogeometric shell: the Reissner–Mindlin shell. *Comput Meth Appl Mech Eng*. 2010;199(5–8):276-289.
- De Luycker E, Benson D, Belytschko T, Bazilevs Y, Hsu M. X-FEM in isogeometric analysis for linear fracture mechanics. *Int J Numer Methods Eng*. 2011;87(6):541-565.
- Beer G. *Advanced Numerical Simulation Methods: From CAD Data Directly to Simulation Results*. London, UK: CRC press; 2015.
- Simpson R, Bordas S, Trevelyan J, Rabczuk T. A two-dimensional isogeometric boundary element method for elastostatic analysis. *Comput Meth Appl Mech Eng*. 2012;209-212:87-100.
- Lian H, Simpson RN, Bordas S. Stress analysis without meshing: isogeometric boundary-element method. *Eng Comput Mech*. 2013;166(2):88-99.
- Scott M, Simpson R, Evans J, et al. Isogeometric boundary element analysis using unstructured T-splines. *Comput Meth Appl Mech Eng*. 2013;254:197-221.
- Seo Y-D, Kim H-J, Youn S-K. Shape optimization and its extension to topological design based on isogeometric analysis. *Int J Solids Struct*. 2010;47(11):1618-1640.
- Lian H, Kerfriden P, Bordas SPA. Implementation of regularized isogeometric boundary element methods for gradient-based shape optimization in two-dimensional linear elasticity. *Int J Numer Methods Eng*. 2016;106(12):972-1017.
- Lian H, Kerfriden P, Bordas SPA. Shape optimization directly from CAD: an isogeometric boundary element approach using T-splines. *Comput Meth Appl Mech Eng*. 2017;317:1-41.
- Peng X, Atroshchenko E, Kerfriden P, Bordas S. Linear elastic fracture simulation directly from CAD: 2D NURBS-based implementation and role of tip enrichment. *Int J Fract Mech*. 2016;204(1):55-78.
- Peng X. Isogeometric Boundary Element Methods for Linear Elastic Fracture Mechanics. Technical Report. Luxembourg City, Luxembourg: University of Luxembourg; 2016. <http://orbilu.uni.lu/handle/10993/25835>
- Peng X, Atroshchenko E, Kerfriden P, Bordas S. Isogeometric boundary element methods for three dimensional static fracture and fatigue crack growth. *Comput Meth Appl Mech Eng*. 2017;316:151-185.
- Beer G, Duenser C. Advanced boundary element analysis of geotechnical problems with geological inclusions. *Comput Geotech*. 2016;79:86-95.

17. Simpson R, Scott M, Taus M, Thomas D, Lian H. Acoustic isogeometric boundary element analysis. *Comput Meth Appl Mech Eng*. 2014;269:265-290.
18. Khajah T, Antoine X, Bordas S. Isogeometric finite element analysis of time-harmonic exterior acoustic scattering problems; 2016. <https://arxiv.org/abs/1610.01694>
19. Buffa A, Sangalli G, Vázquez R. Isogeometric analysis in electromagnetics B-splines approximation. *Comput Meth Appl Mech Eng*. 2010;199(17):1143-1152.
20. Nguyen VP, Anitescu C, Bordas SP, Rabczuk T. Isogeometric analysis: an overview and computer implementation aspects. *Math Comput Simul*. 2015;117:89-116.
21. Lian H, Bordas S, Sevilla R, Simpson R. Recent developments in CAD/analysis integration; 2012. <https://arxiv.org/abs/1210.8216>
22. Nguyen VP, Kerfriden P, Brino M, Bordas SP, Bonisoli E. Nitsche's method for two and three dimensional NURBS patch coupling. *Comput Mech*. 2014;53(6):1163-1182.
23. Coox L, Greco F, Atak O, Vandepitte D, Desmet W. A robust patch coupling method for NURBS-based isogeometric analysis of non-conforming multipatch surfaces. *Comput Meth Appl Mech Eng*. 2017;316(1):235-260.
24. Du X, Zhao G, Wang W. Nitsche method for isogeometric analysis of Reissner-Mindlin plate with non-conforming multi-patches. *Comput Aided Geom Des*. 2015;35:121-136.
25. Xu G, Mourrain B, Duvigneau R, Galligo A. Analysis-suitable volume parameterization of multi-block computational domain in isogeometric applications. *Comput Aided Geom Des*. 2013;45(2):395-404.
26. Schillinger D, Dede L, Scott M, et al. An isogeometric design-through-analysis methodology based on adaptive hierarchical refinement of NURBS, immersed boundary methods, and T-spline CAD surfaces. *Comput Meth Appl Mech Eng*. 2012;249-252:116-150.
27. Marussig B, Zechner J, Beer G, Fries T-P. Fast isogeometric boundary element method based on independent field approximation. *Comput Meth Appl Mech Eng*. 2015;284:458-488.
28. Beer G, Marussig B, Zechner J. A simple approach to the numerical simulation with trimmed CAD surfaces. *Comput Meth Appl Mech Eng*. 2015;285:776-790.
29. Beer G, Marussig B, Zechner J, Dünser C, Fries T-P. Isogeometric boundary element analysis with inclusions. Part 1: Plane problems. *Comput Meth Appl Mech Eng*. 2016;308:552-570.
30. Beer G, Mallardo V, Ruocco E, et al. Isogeometric boundary element analysis with elasto-plastic inclusions. Part 2: 3-D, problems. *Comput Meth Appl Mech Eng*. 2017;315:418-433.
31. Beer G, Mallardo V, Ruocco E, Dünser C. Isogeometric boundary element analysis of steady incompressible viscous flow, Part 1: Plane problems. *Comput Meth Appl Mech Eng*. 2017;326C:51-69.
32. Li X, Chen F, Kang H, Deng J. A survey on the local refinable splines. *Sci China Math*. 2016;59(4):617-644.
33. Forsey DR, Bartels RH. Hierarchical B-spline refinement. *SIGGRAPH Comput Graph*. 1988;22(4):205-212.
34. Vuong A-V, Giannelli C, Jüttler B, Simeon B. A hierarchical approach to adaptive local refinement in isogeometric analysis. *Comput Meth Appl Mech Eng*. 2011;200(49-52):3554-3567.
35. Giannelli C, Jüttler B, Speleers H. THB-splines: the truncated basis for hierarchical splines. *Comput Aided Geom Des*. 2012;29(7):485-498.
36. Giannelli C, Jüttler B, Kleiss S, Mantzaflaris A, Simeon B, Špeh J. THB-splines: an effective mathematical technology for adaptive refinement in geometric design and isogeometric analysis. *Comput Meth Appl Mech Eng*. 2016;299:337-365.
37. Sederberg T, Zheng J, Bakenov A, Nasri A. T-splines and T-NURCCs. *ACM Trans Graph*. 2003;22(3):477-484.
38. Sederberg T, Cardon D, Finnigan G, North N, Zheng J, Lyche T. T-spline simplification and local refinement. *ACM Trans Graph*. 2004;23(3):276-283.
39. Beirão da Veiga L, Buffa A, Sangalli G, Vázquez R. Analysis-suitable T-splines of arbitrary degree: definition, linear independence and approximation properties. *Math Model Meth Appl Sci*. 2013;23(11):1979-2003.
40. Bressan A, Buffa A, Sangalli G. Characterization of analysis-suitable T-splines. *Comput Aided Geom Des*. 2015;39:17-49.
41. Beirão da Veiga L, Buffa A, Cho D, Sangalli G. Isogeometric analysis using T-splines on two-patch geometries. *Comput Meth Appl Mech Eng*. 2011;200(21):1787-1803.
42. Zhang J, Li X. On degree elevation of T-splines. *Comput Aided Geom Des*. 2016;46:16-29.
43. Scott M, Li X, Sederberg T, Hughes T. Local refinement of analysis-suitable T-splines. *Comput Meth Appl Mech Eng*. 2012;213:206-222.
44. Deng J, Chen F, Li X, et al. Polynomial splines over hierarchical T-meshes. *Graph Model*. 2008;70(4):76-86.
45. Nguyen-Thanh N, Nguyen-Xuan H, Bordas S, Rabczuk T. Isogeometric analysis using polynomial splines over hierarchical T-meshes for two-dimensional elastic solids. *Comput Meth Appl Mech Eng*. 2011;200(21-22):1892-1908.
46. Wang P, Xu J, Deng J, Chen F. Adaptive isogeometric analysis using rational PHT-splines. *Comput Aided Des*. 2011;43(11):1448-1438.
47. Toshniwal D, Speleers H, Hughes T. Smooth cubic spline spaces on unstructured quadrilateral meshes with particular emphasis on extraordinary points: geometric design and isogeometric analysis considerations. *Comput Meth Appl Mech Eng*. 2017. <https://doi.org/10.1016/j.cma.2017.06.008>
48. Reif U. A refineable space of smooth spline surfaces of arbitrary topological genus. *J Approx Theory*. 1997;90:174-199.
49. Nguyen T, Peters J. Refinable  $C^1$  spline elements for irregular quad layout. *Comput Aided Geom Des*. 2016;43:123-130.
50. Stummel F. The limitations of the patch test. *Int J Numer Methods Eng*. 1980;15:177-188.
51. Piegl L, Tiller W. *The NURBS Book*. Berlin, Germany: Springer; 1997.
52. Zienkiewicz O, Taylor R, Zhu J. *The Finite Element Method: Its Basis and Fundamentals*. Waltham, MA: Elsevier; 2013.



53. Bazilevs Y, Beirão da Veiga L, Cottrell JA, Hughes TJR, Sangalli G. Isogeometric analysis: approximation, stability and error estimates for  $h$ -refined meshes. *Math Model Meth Appl Sci*. 2006;16(07):1031-1090.
54. Ainsworth M, Oden J. *A Posteriori Error Estimation in Finite Element Analysis*. Toronto, Canada: Wiley Interscience; 2000.

**How to cite this article:** Atroshchenko E, Tomar S, Xu G, Bordas SPA. Weakening the tight coupling between geometry and simulation in isogeometric analysis: From sub- and super-geometric analysis to Geometry-Independent Field approximation (GIFT). *Int J Numer Methods Eng*. 2018;114:1131-1159. <https://doi.org/10.1002/nme.5778>

## APPENDIX A

### PHT-SPLINES

In the GIFT framework with PHT-splines, the computational domain is in the NURBS space, whereas the numerical solution is in the PHT-spline form. Firstly, we construct the parametric domain of the PHT-spline model to represent the numerical solution. We then get the initial numerical solution by solving for the unknown control variables, as presented in Section 2. Then, by using an a posteriori error estimation technique, the supporting cell with large errors in the numerical solution (in the parametric domain) are marked, and the local  $h$ -refinement is performed only on the numerical solution. Several local refinement steps can be performed until the desired error level is achieved.

#### A.1 | Construction of a common parametric domain for NURBS geometry and PHT-spline solution

As a first step, we need to construct a parametric domain of the numerical solution from the given NURBS geometry parameterization. This can be seen as a preprocessing stage. Depending on the parametric domain of the NURBS patches under consideration, two kinds of operations are proposed in this step.

- If the computational domain is made of a single NURBS patch (Figure A1(A)), or multipatches in which the parametric domain of each patch forms a quad-mesh as presented in Figure A1(B), then the parametric domain of the numerical solution is constructed as the partition mesh formed by the knot lines on the parametric domain of the NURBS patches.
- For other cases, such as the examples shown in Figure A1(C), we need to construct the initial parametric mesh  $\mathbb{T}$  according to the topological connection information of the NURBS patches. A reparameterization operation should be performed in this case as described below.

Here, we present an example to show the reparameterization method. Suppose that the patch  $\mathbf{S}_1(u, v)$  in Figure A1(C) has parametric domain  $\mathcal{P}_1 = [a_1, b_1] \times [c_1, d_1]$ , the patch  $\mathbf{S}_2(u, v)$  has parametric domain  $\mathcal{P}_2 = [a_1, b_1] \times [c_2, d_2]$ , and the patch  $\mathbf{S}_3(u, v)$  has parametric domain  $\mathcal{P}_3 = [a_3, b_3] \times [c_1, d_1]$ . Then, according to the topological information of all three patches, the parametric domain for the PHT-spline numerical solution should be constructed as shown in Figure A1(C). In other words, the parametric domain of  $\mathbf{S}_1(u, v)$  does not change, whereas the parametric domain of  $\mathbf{S}_2(u, v)$  changes to  $[a_1, b_1] \times [d_1, d_1 + (d_2 - c_2)]$  and the parametric domain of  $\mathbf{S}_3(u, v)$  changes to  $[b_1, b_1 + (b_3 - a_3)] \times [c_1, d_1]$ .

In order to maintain the geometry of the patches during the transformation of the parametric domain, a reparameterization technique should be adopted to obtain the new parametric representation of each patch. Suppose that the initial parametric domain of  $\mathbf{S}(u, v)$  is  $[a, b] \times [c, d]$ , we can then use the following parameter transformation to achieve a new parameterization  $\mathbf{F}(\xi, \eta)$  with parametric domain  $[e, f] \times [g, h]$ :

$$u(\xi, \eta) = \frac{1}{f - e} [(f - \xi)a + (\xi - e)b] \quad (\text{A1})$$

$$v(\xi, \eta) = \frac{1}{h - g} [(h - \eta)c + (\eta - g)d]. \quad (\text{A2})$$

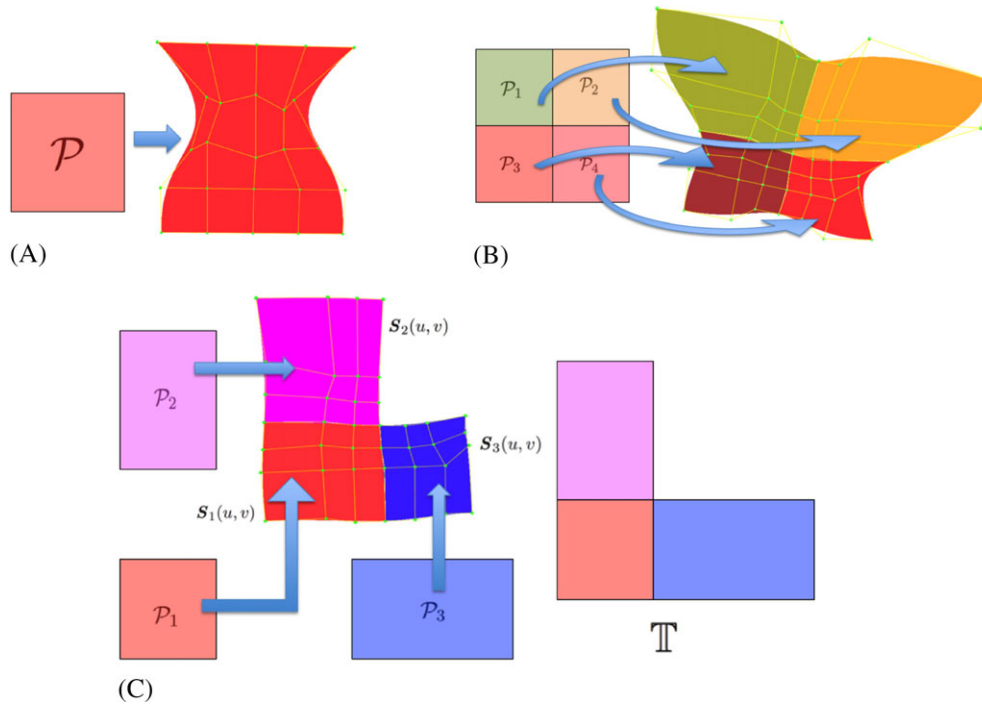


**FIGURE A1** Parametric T-mesh  $\mathbb{T}$  construction for Geometry-Independent Field approximation with PHT-splines. A, Case of a single nonuniform rational B-splines patch; B, Case of multipatch in which the parametric domain of each patch forms a quad-mesh; C, Other cases in which reparameterization is required [Colour figure can be viewed at [wileyonlinelibrary.com](http://wileyonlinelibrary.com)]

*Remark 2.* There is actually no need to derive the explicit parametric representation of the reparameterized surface  $F(\xi, \eta)$ . The derivative information required in the solving stage, as shown in (15), can be evaluated from the original parameterization  $S(u, v)$  through the Jacobian transformation matrix.

### A.2 | Residual-based error indicator

Suppose that  $u_h$  is the PHT-spline solution of the problem (9) and (14) by using the GIFT method, and  $u$  is the exact solution. Let  $e_h = u - u_h$  be the error of the GIFT approximation  $u_h$ . As the refinement operation in GIFT is only performed on the numerical solution, in order to determine the parametric cell to be refined, it is required to give an error indicator on each cell of the T-mesh in the parametric domain of the numerical solution.

Suppose that  $\mathcal{K}$  is the cell on the T-mesh  $\mathbb{T}$  of the parametric domain  $\mathcal{P}$  for the PHT-splines solution  $u_h$ . Following the work of Ainsworth and Oden,<sup>54</sup> the residual-based a posteriori error estimate  $\|e_h\|_{\mathcal{P}}^2$  over the parametric domain  $\mathcal{P}$  can be rewritten as follows:

$$\|e_h\|_{\mathcal{P}}^2 \leq C \sum_{\mathcal{K} \in \mathbb{T}} h_{\mathcal{K}}^2 \|f(\mathbf{x}) + \Delta u_h(\mathbf{x})\|_{L^2(\mathcal{K})}^2, \tag{A3}$$

where  $\mathbf{x} = F(\xi, \eta) = (x(\xi, \eta), y(\xi, \eta))$ ,  $C$  is a positive constant, and  $h_{\mathcal{K}}$  is the circumference of the subpatch in the NURBS parameterization  $F(\xi, \eta)$  of  $\Omega$  with respect to the cell  $\mathcal{K}$  in  $\mathcal{P}$ .

From (A3), we can obtain the local error indicator  $e_{\mathcal{K}}$  on each parametric cell  $\mathcal{K}$  as follows:

$$e_{\mathcal{K}} = h_{\mathcal{K}} \|f(\mathbf{x}) + \Delta u_h(\mathbf{x})\|_{L^2(\mathcal{K})}. \tag{A4}$$

If the parametric cell  $\mathcal{K}$  is written as  $[\xi_0, \xi_1] \times [\eta_0, \eta_1]$ , then we have

$$h_{\mathcal{K}} = \int_{\xi_0}^{\xi_1} \Gamma_{\xi}(\xi, \eta_0) d\xi + \int_{\xi_0}^{\xi_1} \Gamma_{\xi}(\xi, \eta_1) d\xi + \int_{\eta_0}^{\eta_1} \Gamma_{\eta}(\xi_0, \eta) d\eta + \int_{\eta_0}^{\eta_1} \Gamma_{\eta}(\xi_1, \eta) d\eta, \tag{A5}$$

where

$$\Gamma_{\xi}(\xi, \eta) = \sqrt{\left(\frac{\partial x}{\partial \xi}\right)^2 + \left(\frac{\partial y}{\partial \xi}\right)^2}, \quad \Gamma_{\eta}(\xi, \eta) = \sqrt{\left(\frac{\partial x}{\partial \eta}\right)^2 + \left(\frac{\partial y}{\partial \eta}\right)^2}. \tag{A6}$$

### A.3 | Refinement strategy

After  $e_{\mathcal{K}}$  is evaluated for each element  $\mathcal{K}$ , the elements are sorted in descending order with respect to  $e_{\mathcal{K}}$ . Then, the first 20% of sorted elements are marked for refinement. In other words, we refine 20% of elements with the biggest  $e_{\mathcal{K}}$ .

## APPENDIX B

### GEOMETRY AND FIELD PARAMETERIZATIONS USED IN THE NUMERICAL EXAMPLES

**TABLE B1** Control points and weights for coarsest parameterization  $Q_0$

$(i,j)$	$P_{ij}^{Q_0,x}$	$P_{ij}^{Q_0,y}$	$w_{ij}^{Q_0}$
(1,1)	1.0000	0.0000	1.0000
(1,2)	1.0000	1.0000	0.7071
(1,3)	0.0000	1.0000	1.0000
(2,1)	2.0000	0.0000	1.0000
(2,2)	2.0000	2.0000	0.7071
(2,3)	0.0000	2.0000	1.0000

**TABLE B2** Control points and weights for parameterization  $A_1$

$(i,j)$	$P_{ij}^{A_1,x}$	$P_{ij}^{A_1,y}$	$w_{ij}^{A_1}$
(1,1)	1.0000	0.0000	1.0000
(1,2)	1.0000	0.0917	0.9634
(1,3)	0.8320	1.0000	0.7437
(1,4)	0.0000	1.0000	1.0000
(2,1)	1.6667	0.0000	1.0000
(2,2)	1.6667	0.1529	0.9634
(2,3)	1.3865	1.6667	0.7437
(2,4)	0.0000	1.6667	1.0000
(3,1)	2.0000	0.0000	1.0000
(3,2)	2.0000	0.1835	0.9634
(3,3)	1.6639	2.0000	0.7437
(3,4)	0.0000	2.0000	1.0000

**TABLE B3** Control points and weights for parameterization  $B_1$

$(i,j)$	$P_{ij}^{B_1,x}$	$P_{ij}^{B_1,y}$	$w_{ij}^{B_1}$
(1,1)	1.0000	0.0000	1.0000
(1,2)	1.0000	0.7509	0.7628
(1,3)	0.1423	1.0000	0.9444
(1,4)	0.0000	1.0000	1.0000
(2,1)	1.1700	0.0000	1.0000
(2,2)	1.1700	0.8786	0.7628
(2,3)	0.1665	1.1700	0.9444
(2,4)	0.0000	1.1700	1.0000
(3,1)	2.0000	0.0000	1.0000
(3,2)	2.0000	1.5018	0.7628
(3,3)	0.2845	2.0000	0.9444
(3,4)	0.0000	2.0000	1.0000

**TABLE B4** Control points and weights for parameterization  $C_1$ 

$(i,j)$	$P_{ij}^{C_1,x}$	$P_{ij}^{C_1,y}$	$w_{ij}^{C_1}$
(1,1)	1.0000	0.0000	1.0000
(1,2)	1.0000	0.0917	0.9634
(1,3)	0.8320	1.0000	0.7437
(1,4)	0.0000	1.0000	1.0000
(2,1)	1.6667	0.0000	1.0000
<b>(2,2)</b>	<b>1.1000</b>	<b>0.3000</b>	<b>0.8000</b>
<b>(2,3)</b>	<b>0.7500</b>	<b>1.4000</b>	<b>0.7500</b>
(2,4)	0.0000	1.6667	1.0000
(3,1)	2.0000	0.0000	1.0000
(3,2)	2.0000	0.1835	0.9634
(3,3)	1.6639	2.0000	0.7437
(3,4)	0.0000	2.0000	1.0000

**TABLE B5** Control points and weights for parameterization  $D_1$ 

$(i,j)$	$P_{ij}^{D_1,x}$	$P_{ij}^{D_1,y}$	$w_{ij}^{D_1}$
(1,1)	1.0000	0.0000	1.0000
(1,2)	1.0000	0.0917	1.0000
(1,3)	0.8320	1.0000	1.0000
(1,4)	0.0000	1.0000	1.0000
(2,1)	1.6667	0.0000	1.0000
(2,2)	1.6667	0.1529	1.0000
(2,3)	1.3865	1.6667	1.0000
(2,4)	0.0000	1.6667	1.0000
(3,1)	2.0000	0.0000	1.0000
(3,2)	2.0000	0.1835	1.0000
(3,3)	1.6639	2.0000	1.0000
(3,4)	0.0000	2.0000	1.0000

**TABLE B6** Control points in the parameterization of Example 4

$(i,j)$	$P_{ij}^x$	$P_{ij}^y$	$w_{ij}$
(1,1)	1.0000	0.0000	1.0000
(1,2)	1.0000	0.4142	0.8536
(1,3)	0.4142	1.0000	0.8536
(1,4)	0.0000	1.0000	1.0000
(2,1)	2.5000	0.0000	1.0000
(2,2)	2.5000	1.5000	0.8000
(2,3)	1.5000	2.5000	0.8000
(2,4)	0.0000	2.5000	1.0000
(3,1)	4.0000	0.0000	1.0000
(3,2)	4.0000	4.0000	1.0000
(3,3)	4.0000	4.0000	1.0000
(3,4)	0.0000	4.0000	1.0000

**TABLE B7** Control points for the parameterization of one-eighth of a sphere

$(i, j, k)$	$P_{ij}^x$	$P_{ij}^y$	$P_{ij}^z$	$w_{ij}$
(1,1,1)	1.0000	0.0000	0.0000	1.0000
(1,2,1)	1.0000	1.0000	0.0000	0.7071
(1,3,1)	0.0000	1.0000	0.0000	1.0000
(2,1,1)	2.0000	0.0000	0.0000	1.0000
(2,2,1)	2.0000	2.0000	0.0000	0.7071
(2,3,1)	0.0000	2.0000	0.0000	1.0000
(1,1,2)	1.0000	0.0000	1.0000	0.7071
(1,2,2)	1.0000	1.0000	1.0000	0.5000
(1,3,2)	0.0000	1.0000	0.0000	0.7071
(2,1,2)	2.0000	0.0000	2.0000	0.7071
(2,2,2)	2.0000	2.0000	2.0000	0.5000
(2,3,2)	0.0000	2.0000	0.0000	0.7071
(1,1,3)	0.0000	0.0000	1.0000	1.0000
(1,2,3)	0.0000	1.0000	1.0000	0.7071
(1,3,3)	0.0000	1.0000	0.0000	1.0000
(2,1,3)	0.0000	0.0000	2.0000	1.0000
(2,2,3)	0.0000	2.0000	2.0000	0.7071
(2,3,3)	0.0000	2.0000	0.0000	1.0000